

# 1 Shear capacity of cold-formed steel channels with edge-stiffened web holes, 2 un-stiffened web holes and plain webs

3 Boshan Chen<sup>1</sup>, Krishanu Roy<sup>2\*</sup>, Zhiyuan Fang<sup>3</sup>, Asraf Uzzaman<sup>4</sup>, Cao Hung Pham<sup>5</sup>, Gary M. Raftery<sup>6</sup>, James B.P.  
4 Lim<sup>7</sup>

5 <sup>1</sup> Ph.D. Student, Dept. of Civil and Environmental Engineering, Univ. of Auckland, Auckland, New Zealand.

6 ORCID: <https://orcid.org/0000-0001-9176-0731>. Email: [bche719@aucklanduni.ac.nz](mailto:bche719@aucklanduni.ac.nz)

7 <sup>2</sup> Lecturer, Dept. of Civil and Environmental Engineering, Univ. of Auckland, Auckland, New Zealand

8 ORCID: <https://orcid.org/0000-0002-8086-3070>. Email: [kroy405@aucklanduni.ac.nz](mailto:kroy405@aucklanduni.ac.nz)

9 <sup>3</sup> Ph.D. Student, Dept. of Civil and Environmental Engineering, Univ. of Auckland, Auckland, New Zealand.

10 ORCID: <https://orcid.org/0000-0003-1186-5221>. Email: [zfan995@aucklanduni.ac.nz](mailto:zfan995@aucklanduni.ac.nz)

11 <sup>4</sup> Lecturer, School of Computing, Engineering and Physical Sciences, Univ. of the West of Scotland, United  
12 Kingdom

13 ORCID: <https://orcid.org/0000-0001-9687-5810>. Email: [Asraf.Uzzaman@uws.ac.uk](mailto:Asraf.Uzzaman@uws.ac.uk)

14 <sup>5</sup> Senior lecturer, School of Civil Engineering, The Univ. of Sydney, Australia

15 ORCID: <https://orcid.org/0000-0002-5503-5839>. Email: [caohung.pham@sydney.edu.au](mailto:caohung.pham@sydney.edu.au)

16 <sup>6</sup> Senior Lecturer, Dept. of Civil and Environmental Engineering, Univ. of Auckland, Auckland, New Zealand

17 ORCID: <https://orcid.org/0000-0003-4783-3897>. Email: [g.raftery@auckland.ac.nz](mailto:g.raftery@auckland.ac.nz)

18 <sup>7</sup> Associate Professor, Dept. of Civil and Environmental Engineering, Univ. of Auckland, Auckland, New Zealand.

19 ORCID: <https://orcid.org/0000-0001-9720-8518>. Email: [james.lim@auckland.ac.nz](mailto:james.lim@auckland.ac.nz)

20 \*Corresponding Author Contact Details:

21 Krishanu Roy

22 E: [krishanu.roy@auckland.ac.nz](mailto:krishanu.roy@auckland.ac.nz), T: +64 223917991, F: +64 9 373 7462, Department of Civil Engineering,  
23 University of Auckland, Auckland, New-Zealand-1025

## 24 Abstract

25 In this paper, a total of 254 results comprising 30 shear tests and 224 finite element (FE) analysis  
26 results are reported. Simply supported test specimens of cold-formed steel (CFS) channels with aspect  
27 ratios of 1.0 and 1.5 were tested. For comparison, specimens with un-stiffened web holes and plain  
28 webs were also tested. A nonlinear elasto-plastic FE model was then developed and validated against  
29 the experimental results. Using the validated FE model, a parametric study was conducted to  
30 investigate the effect of various influential parameters on the shear capacity of such CFS channels.  
31 The test and FE results shows that for a channel with edge-stiffened web holes, the shear capacity

32 increased by 13.6% on average, when compared with that of a channel with un-stiffened web holes.  
33 The test and FE results were compared against the design predictions. Upon comparison, it was found  
34 that the design rules of CFS channels with un-stiffened web holes in accordance with the AISI (2016)  
35 and AS/NZS (2018) can be un-conservative by 7%, while calculating the shear capacity of CFS channels  
36 with edge-stiffened web holes. Therefore, a suitable design formula in the form of a shear capacity  
37 reduction factor was proposed for CFS channels with edge-stiffened web holes.

## 38 **Keywords**

39 Cold-formed steel, Channels, Shear capacity, Edge-stiffened web holes, Experiments, Finite element  
40 analysis

## 41 **1 Introduction**

42 In recent times, a new generation of cold-formed steel (CFS) channels with edge-stiffened web holes  
43 developed by Howick Ltd. (2013) are being widely used in New Zealand (Fig. 1). Such CFS channel  
44 members when used as floor joists and bearers are often subjected to concentrated loads, hence  
45 experiencing shear failure. However, no work was reported in the literature investigating the shear  
46 capacity of CFS channels with edge-stiffened web holes. Furthermore, current design codes, i.e., the  
47 American Iron and Steel Institute (AISI) (2016) and the Australian and New Zealand Standards (AS/NZS)  
48 (2018) do not provide any design guidance for CFS channels with edge-stiffened web holes.

49 This paper presents the results of 30 new laboratory tests and 224 finite element analyses (FEA) on  
50 CFS channels with edge-stiffened web holes, un-stiffened web holes, and plain webs when subjected  
51 to shear. Fig. 2. shows the details of the CFS channels studied in this paper.

52 Limited work have been reported in the literature studying CFS channels with edge-stiffened web  
53 holes under different loading cases (Chen et al. 2020a,b, 2021a; Chi et al. 2021). For compression tests,  
54 Chen et al. (2019) experimentally and numerically studied the axial capacity of CFS channels with edge-  
55 stiffened web holes and the results suggested that the axial capacity of CFS channels with edge-

56 stiffened web holes performs better than that of a plain channel. Fang et al. (2021a,b) proposed a  
57 framework of deep belief network (DBN) for studying the axial capacity of CFS channels with edge-  
58 stiffened web holes subject to axial compression. For bending tests, Yu et al. (2012) and Chen et al.  
59 (2020c) studied the influence of edge-stiffened web holes on the moment capacity, and the results  
60 suggested that edge-stiffened web holes can improve the moment capacity of such channels. In terms  
61 of web crippling tests, a recent study by Uzzaman et al. (2017, 2020a,b) and Chen et al. (2021b)  
62 suggested that edge-stiffened web holes can also improve web crippling strength of such channels.  
63 In terms of CFS plain channels, significant work has been reported in the literature. The shear  
64 behaviour of CFS plain channels was first studied by LaBoube and Yu (1978), and they first proposed  
65 suitable design formulas for calculating the shear capacity of CFS plain channels. A study by Keerthan  
66 and Mahendran (2015) found that design shear capacity for CFS plain channels determined from AISI  
67 (2016) and AS/NZS (2018) are conservative as they did not include the post-buckling strength. Hence,  
68 Keerthan and Mahendran (2015) proposed improved shear capacity formulas on the basis of their test  
69 and FEA results. Pham and Hancock (2010a, b) experimentally and numerically studied the shear  
70 behaviour of high strength CFS channels with and without flange straps. They found that the shear  
71 capacities of CFS channels with angle straps are higher than those without flange straps. Also, Pham  
72 and Hancock (2009) found that flanges can have a significant effect on the shear buckling capacity of  
73 CFS channels.

74 Regarding CFS channels with un-stiffened web holes, extensive work has been reported on reduced  
75 shear capacity of CFS channels with un-stiffened web holes by many researchers. Shan et al. (1997)  
76 found that the key parameter for the shear capacity of CFS channels with un-stiffened web holes is  
77 the ratio of the depth of web hole ( $d_{wh}$ ) to clear height of web ( $d_1$ ) and thus developed shear capacity  
78 reduction factors in terms of  $d_{wh}/d_1$ . Eiler (1997) extended the research work of Shan et al. (1997) to  
79 include the effects of web elements with holes when subjected to varying shear force, which have  
80 been adopted in AISI (2016) and AS/NZS (2018). Keerthan and Mahendran (2013b, 2014)

81 experimentally and numerically studied the shear capacity of CFS channels with un-stiffened web  
82 holes. They also used the reduction factor and proposed improved design formulas for such sections.  
83 To extend the direct strength method (DSM) to CFS channels with un-stiffened web holes in shear, an  
84 experimental study was conducted by Pham et al. (2017a, b, 2020a, b, c, d) to study the shear capacity  
85 of CFS channels with un-stiffened web holes having an aspect ratio up to 3.0, and they proposed a  
86 DSM design approach for CFS members with holes in shear. However, no previous research has  
87 studied the shear capacity of CFS channels with edge-stiffened web holes. The issue is addressed in  
88 this paper.

89 As mentioned previously, this paper reports in relation to 30 new laboratory tests on the shear  
90 capacity of CFS channels with edge-stiffened web holes, un-stiffened web holes and plain webs. A  
91 nonlinear FE model was then developed and validated against the results obtained from laboratory  
92 tests in terms of ultimate strength and deformed shapes. A parametric study involving 224 models  
93 was conducted based on the validated FE models. To verify the accuracy of current design procedures  
94 found in the literature for CFS channels with un-stiffened web holes, the results obtained from  
95 laboratory tests and FEA were compared against design predictions of AISI (2016), AS/NZS (2018),  
96 Keerthan and Mahendran (2014), and Shan et al. (1997). Finally, a suitable design formula in the form  
97 of shear capacity reduction factor was proposed for determining the shear capacity of such CFS  
98 channels.

## 99 **2 Experimental study**

### 100 **2.1 Test specimens**

101 A total of 30 CFS channels in shear were studied in this laboratory tests. Six experiments were  
102 conducted on specimens without web holes (Fig.3 (a)), 12 experiments were on specimens with un-  
103 stiffened web holes (Fig.3 (b)) and the remaining 12 experiments were conducted on specimens with  
104 edge-stiffened web holes (Fig.3 (c)).

105 To simulate shear boundary conditions, relatively short test beams having two aspect ratios (shear  
106 span /clear web height ( $d_1$ )) of 1.0 and 1.5 were selected. This paper mainly focused on the shear  
107 behaviour of such CFS channel sections with a shear span-to-clear web height ratio of 1.0. However,  
108 the influence of combined shear and bending behaviour on the strength and failure modes of such  
109 sections were also experimentally investigated (aspect ratios of 1.5).

110 The test specimens comprised two different section sizes, namely section 240 and section 290. To  
111 study the influence of hole sizes on the shear capacity of CFS channels, two different hole diameters  
112 ( $d_{wh}$ ) of 90 and 140 mm were selected.

113 It should be noted that the web holes are strengthened through a continuous lip around the perimeter  
114 of the hole (i.e., with edge-stiffened web hole). As can be seen from Fig.2, the length of the edge-  
115 stiffener was fixed at 13 mm. Tables 1 and 2 summarise the measured dimensions of test specimens.

## 116 **2.2 Section labels**

117 The test specimens were labelled in such a way that the nominal dimensions of web depth, aspect  
118 ratio, diameter of holes, the type of web holes, and the flange conditions were identified by the label.  
119 For example, the label “240-A1.0-D90-EH-FR” can be interpreted as follows:

- 120 ● “240” means the nominal dimensions of web depth in millimetres i.e.,  $d=240$  mm.
- 121 ● “A1.0” is the aspect ratio of the channel beams i.e.,  $a/d_1=1.0$
- 122 ● “D90” means the nominal diameter of web holes in millimetres i.e.,  $d_{wh} = 90$  mm.
- 123 ● “EH’ identifies a web with edge-stiffened hole, “NH’ identifies a plain web, and “UH’ means a  
124 web with un-stiffened hole.
- 125 ● “FR” represents the flanges restrained by flange straps.

## 126 **2.3 Material testing**

127 To obtain the material properties of the test specimens, a total of 6 coupons were prepared, which  
128 were cut from the flat portion of the channels, and tested using an Instron tensile testing machine in  
129 accordance with the test procedure mentioned in the ISO 6892-1 (ISO 2009) (Fig. 4). The stress-strain

130 curves obtained from the tensile coupon tests for sections 240 and 290 are presented in Figs. 5(a) and  
131 (b), respectively. Table 3 shows that the average yield stresses ( $\sigma_{0.2}$ ) for section 240 and 290 are 301.6  
132 MPa and 308.5 MPa, respectively.

#### 133 **2.4 Testing-rig and loading procedure**

134 The concentrated loads were applied using an MTS machine with a capacity of 300 kN at a constant  
135 rate of 0.7 mm/min. Two single channels were connected back-to-back by using three numbers of  
136 30mm thick T-shaped stiffeners. The use of twelve 100-mm-wide stiffening plates during the tests was  
137 to provide the required simply supported boundary conditions at the supports and at the loading  
138 point, while also eliminating the possibility of web crippling failure. A 30-mm gap was incorporated  
139 between the two specimens to allow the test beams to buckle independently. To study the influence  
140 of flange straps on the shear behaviour and strength, 20 tests were conducted on restrained supports,  
141 which were ensured by using eight angle straps at the loading and support points. Additionally, 10  
142 tests were conducted without using any angle strap. Three linear variable differential transformers  
143 (LVDTs) were selected to record the vertical displacement of the test specimens. One LVDT was placed  
144 under the loading point while the remaining two LVDTs were placed at the support point. The  
145 photograph and schematic drawing of the experimental setup are presented in Figs. 6. and 7.,  
146 respectively.

#### 147 **2.5 Experimental results**

148 Fig. 8. plotted the shear capacity versus displacement curves of all test specimens. The shear capacity  
149 was determined as the applied load ( $P$ ) divided by four, as two back-to-back CFS channels were used.  
150 Fig. 9. shows the deformed shapes of the CFS channels with flange straps. From the failure modes, it  
151 can be clearly seen that shear failure occurred for all test specimens. The ultimate shear capacity ( $V_u$ )  
152 obtained from the laboratory tests are summarized in Tables 1 and 2 for fastened flange and  
153 unfastened flange cases, respectively. As shown in Tables 1 and 2, for a channel with edge-stiffened

154 web holes, the shear capacity increased by 13.6% on average, when compared with that of a channel  
155 with un-stiffened web holes.

156 Table 4 summarizes the shear capacity of CFS channels with and without flange straps (i.e., with and  
157 without flange restraints). From the results reported in Table 4, it can be confirmed that there is a  
158 reduction in shear capacity of CFS channels by 11.04% on average, when the straps were not attached  
159 to their flanges. Fig. 10 shows the failure modes of CFS plain channels, when the flanges were not  
160 restrained (without flange straps). It can be seen that the flange distortions occurred due to the  
161 distortional buckling or unbalanced shear flow in these sections.

162 The combined shear and bending behaviour can significantly affect the shear capacity for those longer  
163 specimens having higher aspect ratios. Table 5 shows the comparison of the shear capacity of  
164 specimens having aspect ratios of 1.0 and 1.5. This comparison indicates that shear capacities of those  
165 specimens having an aspect ratio of 1.5 were reduced by 24.9% on average due to this combined shear  
166 and bending action.

### 167 **3 Numerical study**

#### 168 **3.1 General**

169 ABAQUS (2018) software was used to develop a nonlinear FE model to simulate the CFS channels with  
170 and without holes in shear. The measured cross-section dimensions as well as material properties  
171 obtained from the tensile coupon tests were incorporated in the FE model. Specific modeling  
172 techniques are discussed next.

#### 173 **3.2 Modeling of geometry and material properties**

174 The ABAQUS classical metal plasticity model was selected to define the isotropic yielding and plastic  
175 hardening of the steel. The material properties obtained from the tensile coupon tests were  
176 incorporated in the FE models. A similar modeling technique was used by Roy et al. (2020) and Li et

177 al. (2019). As per the ABAQUS manual (2018), the engineering material curve was converted into a  
178 true material curve by using the following formulas given below:

$$\sigma_{true} = \sigma(1 + \varepsilon) \quad (1)$$

$$\varepsilon_{true(pl)} = \ln(1 + \varepsilon) - \frac{\sigma_{true}}{E} \quad (2)$$

### 179 **3.3 FE meshing**

180 S4R shell elements were selected to model the CFS channels. The mesh sensitivity analysis indicated  
181 that a mesh size between 5 mm to 10 mm was selected for modeling the CFS channels with and  
182 without web holes. For the T-shaped stiffeners, a mesh size of 10 mm × 10 mm was selected. Mesh  
183 refinement was selected around the web holes and rounded corners to enable an accurate FE analysis  
184 (Fig. 11).

### 185 **3.4 Boundary conditions and loading procedure**

186 The simply supported boundary conditions were modelled by releasing both the in-plane rotation and  
187 axial displacement. The reference points were placed at the top of T-shaped stiffeners. The vertical  
188 translation was not restrained at the loading point. The vertical loading was applied by specifying the  
189 displacement at the reference loading points. In the FE model, surface-to-surface interaction was used  
190 between the webs of each CFS channel. It should be noted that the modeling of bolting connections  
191 was simplified to eliminate any possible slippage of the bolts. The experimental results confirmed that  
192 the failure of angle straps did not occur when they were used in the tests. Therefore, the angle straps  
193 were simulated using suitable boundary conditions. The applied boundary conditions in the FE model  
194 are presented in Fig. 12 for the specimen 290-A1.5-D140-EH-FR.

### 195 **3.5. Modeling of initial geometric imperfections and residual stresses**

196 It should be noted that a value of  $0.006d_1$  was taken as the magnitude of imperfections in the  
197 numerical modeling of CFS channels (Keerthan and Mahendran 2014). The imperfect initial geometries  
198 were simulated using the \*IMPERFECTION option in the ABAQUS (2018) library. From analysing a



199 limited number of FE models, a decrease of only 1.2% in shear capacity was found when the effects of  
200 residual stresses were considered in the FE models, indicating that residual stresses have negligible  
201 effect on the shear capacity of CFS channels (Fig. 13). Therefore, the influence of residual stresses on  
202 the shear capacity of CFS channels was not considered in the FE models.

### 203 **3.6 Validation of the finite element model**

204 Table 6 reports the comparison of the laboratory test results ( $V_{EXP}$ ) with the numerical results ( $V_{FEA}$ ).  
205 The mean value of the  $V_{EXP} / V_{FEA}$  ratio is 1.01 with the corresponding coefficient of variation (COV) of  
206 0.07. Fig. 14 presents the deformed shapes at failure from both the laboratory tests and FEA. It can be  
207 clearly seen that the deformed shapes determined from the FEA are similar to those determined from  
208 the laboratory tests. Fig. 15 plotted shear capacity versus displacement behaviour obtained from both  
209 the FEA and laboratory tests for specimens 240-A1.5-D90-UH-FR and 240-A1.5-D90-UH-FU, which  
210 shows good agreement between FEA and laboratory test results.

## 211 **4 Parametric study**

212 A parametric study comprising 224 FE models was undertaken to develop an extensive shear capacity  
213 database for CFS channels with edge-stiffened web holes, un-stiffened web holes and plain webs. It  
214 should be noted that only aspect ratios of 1.0 were considered in the parametric study section, as the  
215 parametric study section only considered the shear behaviour of such sections.

216 To investigate the influence of web height to web thickness ratio ( $d_1/t_w$ ) on the shear capacity of such  
217 sections, the same FE model was selected with varying web thickness ( $t_w$ ). The  $d_1/t_w$  ratio was thus  
218 varied from 96 to 290 by varying the web thickness from 1.0 mm to 2.5 mm, as listed in Table 7. For  
219 specimens with holes, the ratio of  $d_{wh}/d_1$  was varied between 0.1 and 0.7 to investigate the influences  
220 of hole diameter on the shear capacity of such sections. The ratio of stiffener length to web height  
221 ( $q/d_1$ ) was changed from 0.04 to 0.12. The FE models in the parametric study were coded in such a  
222 way that all the geometric parameters could be automatically varied.

223 Fig. 16(a) and Table 7 show the influence of  $q/d_1$  ratio on the shear capacity of CFS channels with  
 224 edge-stiffened web holes. The comparison showed that an increase in shear capacity of 11.6% was  
 225 noticed when  $q/d_1$  ratio was increased from 0.04 to 0.12. It was found that the influence of stiffener  
 226 length on the shear capacity of such CFS channels cannot be ignored. Fig. 16(b) and Table 7 show the  
 227 influence of the ratio  $d_{wh}/d_1$  on the shear capacity of CFS channels with edge-stiffened web holes. The  
 228 comparison results indicated that the ultimate shear capacities were decreased by 53% on average  
 229 when  $d_{wh}/d_1$  ratio was changed from 0.1 to 0.7, indicating that the influence of  $d_{wh}/d_1$  ratio on the  
 230 shear capacity of CFS channels was significant.

## 231 **5 Current shear design rules**

### 232 **5.1 General**

233 Current design rules for calculating the shear capacity of CFS channels with holes are designed on the  
 234 basis of a reduction factor ( $q_s$ ), which can be defined as the ratio of nominal shear capacity of CFS  
 235 channels with holes ( $V_n$ ) to the nominal shear capacity of CFS channels without holes ( $V_v$ ). In this  
 236 section, the currently available design rules for calculating the nominal shear capacity of CFS without  
 237 holes ( $V_v$ ) as well as reduction factor ( $q_s$ ) are discussed next.

### 238 **5.2 Design rules for CFS channels without web holes in shear**

#### 239 *5.2.1 DSM design rules in shear without tension field action*

240 According to Section G2.2 of AISI (2016) and Clause 7.2.3 of AS/NZS (2018), the nominal shear capacity  
 241 ( $V_{DSM-1}$ ) of unperforated CFS channel beams without web stiffeners can be calculated using the  
 242 following Equations (3) to (8).

$$V_v = V_y \quad \text{For } \lambda_v \leq 0.815 \quad (3)$$

$$V_v = 0.815 \sqrt{V_{cr} V_y} \quad \text{For } 0.815 < \lambda_v \leq 1.227 \quad (4)$$

$$V_v = V_{cr} \quad \text{For } \lambda_v > 1.227 \quad (5)$$

$$V_y = 0.6A_w F_y \quad (6)$$

$$V_{cr} = \frac{0.904Ek_v t_w^3}{d_1} \quad (7)$$

$$\lambda_v = \sqrt{\frac{V_y}{V_{cr}}} \quad (8)$$

243 *5.2.2 DSM design rules in shear with tension field action*

244 Pham and Hancock (2010a, b) conducted both experimental and numerical investigations to propose  
 245 design formulas for the shear capacity of unperforated CFS channel beams with tension field action  
 246 (Equations 9 and 10), which have been adopted in Section G2.2 of AISI (2016) and in Clause 7.2.3 of  
 247 AS/NZS (2018) standards. These formulas ( $V_{DSM-2}$ ) can closely predict the shear capacity of CFS lipped  
 248 channels without holes, which accounts for their post-buckling strength and includes the influence of  
 249 additional fixity on the web-flange junction point.

$$V_v = V_y \quad \text{For, } \lambda_v \leq 0.776 \quad (9)$$

$$V_v = \left[ 1 - 0.15 \left( \frac{V_{cr}}{V_y} \right)^{0.4} \right] \left( \frac{V_{cr}}{V_y} \right)^{0.4} V_y \quad \text{For, } \lambda_v > 0.776 \quad (10)$$

250 *5.2.3 Design rules proposed by Keerthan and Mahendran (2015)*

251 Keerthan and Mahendran (2015) modified the current shear design rules of AS/NZS 4600 (2018) and  
 252 proposed new formulas as demonstrated in Equations 11, 12 and 13, which include the available post-  
 253 buckling strength of CFS channels and the additional fixity on the web-flange junction point. The shear  
 254 buckling coefficient ( $k_{LCB}$ ) was included to allow for the additional fixity at the web-flange junction of  
 255 CFS channels, while a post-buckling coefficient of 0.2 was selected in Equations 12 and 13, as shown  
 256 below:

$$V_v = V_y \quad \text{For, } \frac{d_1}{t_w} \leq \sqrt{\frac{Ek_{LCB}}{f_y}} \quad (11)$$

$$V_v = V_i + 0.2(V_y - V_i) \quad \text{For, } \sqrt{\frac{Ek_v}{f_y}} < \frac{d_1}{t_w} \leq 1.508 \sqrt{\frac{Ek_{LCB}}{f_y}} \quad (12)$$

$$V_v = V_{cr} + 0.2(V_y - V_{cr}) \quad \text{For, } \frac{d_1}{t_w} \geq 1.508 \sqrt{\frac{Ek_{LCB}}{f_y}} \quad (13)$$

257 **5.3 Design rules for CFS channels with un-stiffened web holes in shear**

258 *5.3.1 Design rules proposed by Shan et al. (1997)*

259 Shan et al. (1997) concluded that the main parameter influencing the shear capacity is the ratio of  
 260 depth of the hole to the flat depth of the web ( $d_{wh}/d_1$ ), and they developed a linear reduction factor  
 261 for CFS channels with un-stiffened web holes, which incorporated the parameter  $d_{wh}/d_1$ . The reduction  
 262 factor proposed by Shan et al. (1997) can be determined by using Equations 14 and 15:

$$q_s = 1.71 - 3.66\left(\frac{d_{wh}}{d_1}\right) \quad \text{For } \frac{d_{wh}}{d_1} < 0.38 \quad (14)$$

$$q_s = 0.46 - 0.38\frac{d_{wh}}{d_1} \quad \text{For } 0.38 < \frac{d_{wh}}{d_1} \leq 1 \quad (15)$$

263 *5.3.2 Design rules in accordance with the design rules of AISI (2016) and AS/NZS (2018)*

264 The formulas for determining the shear capacity reduction factor are presented in AISI (2016) and  
 265 AS/NZS (2018) for CFS channels with un-stiffened web holes on the basis of the research findings of  
 266 Eiler et al. (1997), who suggested that the reduction of shear capacity due to the presence of web  
 267 holes can be estimated by applying a reduction factor to the nominal shear capacity of the plain web.  
 268 The shear capacity reduction factor formulas developed by Eiler et al. (1997), which are available in  
 269 AISI (2016) and AS/NZS (2018) can be determined by using Equations 16 to 20:

$$q_s = 1 \quad \text{For } \frac{c}{t} > 54 \quad (16)$$

$$q_s = \frac{c}{54t} \quad \text{For } 5 < \frac{c}{t} < 54 \quad (17)$$

$$c = \frac{d_1}{2} - \frac{d_{wh}}{2.83} \quad (18)$$

$$\frac{d_{wh}}{d_1} \leq 0.7 \quad (19)$$

$$\frac{d_1}{t} \leq 200 \quad (20)$$

270 *5.3.3 Design rules proposed by Keerthan and Mahendran (2013b, 2014)*

271 Keerthan and Mahendran (2013b, 2014) experimentally and numerically studied the shear capacity of  
 272 CFS channels with un-stiffened web holes. From the outcome of their research, they proposed shear  
 273 capacity reduction factors due to the presence of web holes. Based on their recommendation, shear  
 274 capacity of CFS channels with un-stiffened web holes ( $V_{ni}$ ) can be calculated using a reduction factor  
 275  $q_s$ , which is normally applied to the shear capacity of plain channels ( $V_v$ ). Equations 21 to 23 present  
 276 the proposed design formulas for the shear capacity reduction factor of perforated CFS channel  
 277 sections.

$$q_s = 1 - 0.6\left(\frac{d_{wh}}{d_1}\right) \quad \text{For } 0 < \frac{d_{wh}}{d_1} < 0.3 \quad (21)$$

$$q_s = 1.215 - 1.316\left(\frac{d_{wh}}{d_1}\right) \quad \text{For } 0.3 < \frac{d_{wh}}{d_1} < 0.7 \quad (22)$$

$$q_s = 0.732 - 0.625\left(\frac{d_{wh}}{d_1}\right) \quad \text{For } 0.7 < \frac{d_{wh}}{d_1} < 0.85 \quad (23)$$

## 278 **6. Comparison of tests and FE results with design strengths**

279 The results obtained from laboratory tests and FEA were in comparison with the design shear  
 280 capacities determined from the design rules of AISI (2016), AS/NZS (2018), Pham and Hancock (2010a,  
 281 b) and Keerthan and Mahendran (2015) for CFS plain channels. The comparison results are reported  
 282 in Table 8 and plotted in Fig.17. The DSM design rules in shear without tension field action as per the  
 283 AISI (2016) and AS/NZS (2018), are overly conservative, as they do not include the influence of post-  
 284 buckling strength. However, the DSM design rules in shear with tension field action proposed by Pham  
 285 and Hancock (2010a, b) was close to the results obtained from laboratory tests. The results obtained  
 286 from the formulas proposed by Keerthan and Mahendran (2015) are conservative by 18% on average,  
 287 when compared with the results obtained from the laboratory tests.

288 The shear capacities of CFS channels with un-stiffened web holes obtained from the laboratory tests  
 289 and FEA are in comparison with the predictions from the currently available design rules as shown in  
 290 Table 9. The comparison results show that the shear capacities determined from Shan et al.'s (1997)

291 design formulas are over conservative by 62% on average. The design formulas in accordance with the  
 292 AISI (2016) and AS/NZS (2018) are conservative mostly for CFS channels with small web holes, while  
 293 they are un-conservative for channels with larger web holes, which was also reported by Keerthan and  
 294 Mahendran (2013b, 2014). This comparison shows that the shear capacities determined from  
 295 Keerthan and Mahendran's (2013b, 2014) design formulas are conservative by 7% on average. Fig. 18  
 296 shows the non-dimensional curve of  $q_s$  versus  $d_{wh}/d_1$ .  
 297 For CFS channels with edge-stiffened web holes, the shear capacity reduction factors obtained from  
 298 laboratory tests and FEA were in comparison with those obtained from the design formulas of CFS  
 299 channels with un-stiffened web holes. The comparison results are presented in Table 10, indicating  
 300 that the design formulas in accordance with the AISI (2016) and AS/NZS (2018) are un-conservative by  
 301 7% on average. This is due to the fact that the current design rules of CFS channels with web holes do  
 302 not consider the effects of edge-stiffener. Therefore, new design rules for CFS channels with edge-  
 303 stiffened web holes should be developed.

## 304 **7. Proposed design formulas**

305 New design rules in the form of a reduction factor were proposed in this paper to determine the shear  
 306 capacity of CFS channels with edge-stiffened web holes, based on the experimental and numerical  
 307 results presented herein. It should be noted that a previous study reported by the same authors (Chen  
 308 et al. 2020c) indicated that the influences of  $r_q/t_w$  ratio on the capacity of such CFS channels are  
 309 limited. Therefore, the ratio  $r_q/t_w$  was not considered in the proposed design formulas. Only the  
 310 primary influencing parameters such as,  $q/d_1$  and  $d_{wh}/d_1$  ratios were considered. The design formulas  
 311 for calculating the shear capacity reduction factors ( $q_{s(pr)}$ ) of CFS channels with edge-stiffened web  
 312 holes are given next.

$$q_{s(pr)} = 1.04 + 0.67 \frac{q}{d_1} - 0.59 \frac{d_{wh}}{d_1} \quad \text{For, } 0.1 \leq d_{wh}/d_1 \leq 0.3 \quad (24)$$

$$q_{s(pr)} = 1.42 + 1.08 \frac{q}{d_1} - 1.59 \frac{d_{wh}}{d_1} \quad \text{For, } 0.3 < d_{wh}/d_1 \leq 0.5 \quad (25)$$

$$q_{s(pr)} = 1.72 + 1.18 \frac{q}{d_1} - 1.91 \frac{d_{wh}}{d_1} \quad \text{For, } 0.5 < d_{wh}/d_1 \leq 0.7 \quad (26)$$

313 The validity for the proposed design formulas shall apply within the following limits: (a)  $0.1 \leq d_{wh}/d_1 \leq 0.7$ ;  
 314 (b)  $0.04 \leq q/d_1 \leq 0.12$ ; (c)  $96 \leq d_1/t_w \leq 290$

315 In order to assess the accuracy of the proposed design formulas for a shear capacity reduction factor  
 316 of CFS channels with edge-stiffened web holes (Equations (24)-(26)), Fig. 19 and Table 10 compare  
 317 their predictions with the corresponding results obtained from laboratory tests and FEA. From the  
 318 comparison results, it was found that the shear capacity reduction factor determined from Equations  
 319 (24) to (26) agree well with the results obtained from laboratory tests and FEA.

## 320 **8. Reliability analysis**

321 A reliability analysis was carried out to assess the reliability of the proposed design formulas for  
 322 determining the shear capacity reduction factors of CFS channels with edge-stiffened web holes. A  
 323 target reliability index of 2.5 for CFS structural members is recommended as a lower limit in the AISI  
 324 Specification (2016). Design formulas are considered reliable if the value of the reliability index ( $\beta$ ) is  
 325 greater than or equal to 2.5 (AISI, 2016). A load combination of 1.2DL+1.6LL as specified in the AISI  
 326 Specification (2016) was used in the reliability analysis. In the calculation, DL means the dead load,  
 327 while LL means the live load. The statistical parameters were determined from the AISI Specification  
 328 (2016) for CFS members, where  $M_m = 1.10$ ,  $F_m = 1.00$ ,  $V_M = 0.10$ , and  $V_F = 0.05$ . These values are the  
 329 mean values and coefficients of variations for material and fabrication properties.

330 Table 11 confirms that the values of  $\beta$  are 2.84, 2.80 and 2.80, for Equations 24, 25 and 26,  
 331 respectively, indicating that the proposed design formulas are reliable for determining the shear  
 332 capacity reduction factor of CFS channels with edge-stiffened web holes.

## 333 **9. Concluding remarks**

334 This paper presents the details of an experimental and numerical investigation into the shear capacity  
335 of CFS channels with edge-stiffened web holes, un-stiffened web holes and plain webs. A total of 254  
336 results comprising 30 laboratory tests and 224 FE results are reported.

337 The results obtained from laboratory tests indicate that for a channel with edge-stiffened web holes,  
338 the shear capacity increased by 13.6% on average, when compared with that of a channel with un-  
339 stiffened web holes. Also, CFS channels without flange restraints had an 11.04% lower shear capacity  
340 than its restrained equivalent. The shear capacities of those specimens with an aspect ratio of 1.5  
341 were reduced by 24.9% on average due to this combined action.

342 A numerical model is then developed and validated against the corresponding results obtained from  
343 laboratory tests, which showed good agreement both in terms of ultimate strength and failure modes.

344 A parametric study comprising 224 FE models was conducted based on the validated FE models

345 The current design formulas in AISI (2016) and AS/NZS (2018) for web holes are demonstrated to be  
346 un-conservative by 7% on average when determining the shear capacity reduction factor of such CFS  
347 channels with edge-stiffened web holes.

348 Modified design formulas are therefore proposed using bivariate linear regression analysis. A  
349 reliability analysis was carried out to assess the proposed design formulas, indicating that the  
350 proposed design formulas can closely determine the shear capacity reduction factor of CFS channels  
351 with edge-stiffened web holes.

## 352 **Data Availability Statement**

353 All of the data and models generated or used during the study appear in the submitted article.

## 354 **Acknowledgements**

355 Test specimens were provided by Howick NZ. Ltd. and this is greatly acknowledged by the authors.

356 The shear tests were carried out at University of Auckland.



357 **References**

- 358 ABAQUS version 6.14-2 [Computer software]. Dassault Systemes, Waltham, MA, 2018.
- 359 American Iron and Steel Institute (AISI) 2016. "North American specification for the design of cold-  
360 formed steel structural members, 2016 Edition." AISI S100-16w, Washington, DC. USA.
- 361 Australia/New Zealand Standard (AS/NZS). 2018. "Cold-Formed Steel Structures, AS/NZS 4600:2018."  
362 Joint Technical Committee, Sydney.
- 363 Chen, B., K. Roy, A. Uzzaman, G.M. Raftery, D. Nash, G. C. Clifton, P. Pouladi, and J.B.P. Lim. 2019.  
364 "Effects of edge-stiffened web openings on the behaviour of cold-formed steel channel sections  
365 under compression." *Thin-Walled Struct.* 144:106307.  
366 <https://doi.org/10.1016/j.tws.2019.106307>.
- 367 Chen, B., K. Roy, A. Uzzaman, G.M. Raftery, and J.B.P. Lim. 2020a. "Parametric study and simplified  
368 design equations for cold-formed steel channels with edge-stiffened holes under axial  
369 compression." *J. Constr. Steel Res.*, 172:106161. <https://doi.org/10.1016/j.jcsr.2020.106161>.
- 370 Chen, B., K. Roy, A. Uzzaman, G.M. Raftery, and J.B.P. Lim. 2020b. "Axial strength of back-to-back cold-  
371 formed steel channels with edge-stiffened holes, un-stiffened holes and plain webs" *J. Constr.*  
372 *Steel Res.*, 174:106313. <https://doi.org/10.1016/j.jcsr.2020.106313>.
- 373 Chen, B., K. Roy, A. Uzzaman, and J.B.P. Lim. 2020c. "Moment capacity of cold-formed channel beams  
374 with edge-stiffened web holes, un-stiffened web holes and plain webs." *Thin-Walled Struct.*  
375 157:107070. <https://doi.org/10.1016/j.tws.2020.107070>.
- 376 Chen, B., K. Roy, Z. Fang, A. Uzzaman, G.M. Raftery, and J.B.P. Lim. 2021a. "Moment capacity of back-  
377 to-back cold-formed steel channels with edge -stiffened hole, un-stiffened hole, and plain web"  
378 *Eng. Struct.*, 235:112042. <https://doi.org/10.1016/j.engstruct.2021.112042>.
- 379 Chen, B., K. Roy, Z. Fang, A. Uzzaman, Y. Chi, and J.B.P. Lim. 2021b. "Web crippling capacity of fastened  
380 cold-formed steel channels with edge-stiffened web holes, un-stiffened web holes and plain webs

381 under two-flange loading.” *Thin-Walled Struct.* 163:107666.  
382 <https://doi.org/10.1016/j.tws.2021.107666>.

383 Chi, Y., K. Roy, B. Chen, Z. Fang, A. Uzzaman, and J.B.P. Lim, 2021. “The effect of opening spacing on  
384 the axial capacity of built-up cold-formed steel channel sections with edge-stiffened web holes”  
385 *Steel Compos. Struct.*, 40(2):287-305. <http://dx.doi.org/10.12989/scs.2021.40.2.287>.

386 Eiler, M.R., R. Laboube, and W.W. Yu, 1997. “Behaviour of web elements with openings subjected to  
387 linearly varying shear.” Univ. of Missouri-Rolla, Rolla, USA

388 Fang, Z., K. Roy, B. Chen, C.W. Sham, I. Hajirasouliha, and J.B.P.Lim. 2021a. “Deep learning-based  
389 procedure for structural design of cold-formed steel channel sections with edge-stiffened and un-  
390 stiffened holes under axial compression” *Thin-Walled Struct.* 166:108076.  
391 <https://doi.org/10.1016/j.tws.2021.108076>.

392 Fang, Z., K. Roy, J. Mares, C.W. Sham, B. Chen, and J.B.P.Lim. 2021b. “Deep learning-based axial  
393 capacity prediction for cold-formed steel channel sections using Deep Belief Network” *Struct.* 33:  
394 2792-2802. <https://doi.org/10.1016/j.istruc.2021.05.096>.

395 Howick (2013). Floor joist system. Auckland, New Zealand.

396 ISO E. 6892-1. 2009. “Metallic Materials: Tensile Testing: Part 1: Method of Test at Room  
397 Temperature” ISO E. 6892-1, International Standard, Geneva.

398 Keerthan, P., and M. Mahendran. 2013a. “Shear buckling characteristics of cold-formed steel channel  
399 beams.” *Int J Steel Struct.*,13: 385-399. [https://doi-org.ezproxy.auckland.ac.nz/10.1007/s13296-](https://doi-org.ezproxy.auckland.ac.nz/10.1007/s13296-013-3001-6)  
400 013-3001-6.

401 Keerthan, P., and M. Mahendran. 2013b. “Experimental studies of the shear behaviour and strength  
402 of lipped channel beams with web openings.” *Thin-Walled Struct.*, 73: 131-144.  
403 <https://doi.org/10.1016/j.tws.2013.06.018>.

404 Keerthan, P., and M. Mahendran. 2013c. "New design rules for the shear strength of littesteel beams  
405 with web openings." *J. Struct. Eng.*, 139(5): 640-656. [https://doi.org/10.1061/\(ASCE\)ST.1943-](https://doi.org/10.1061/(ASCE)ST.1943-541X.0000563)  
406 541X.0000563.

407 Keerthan, P., and M. Mahendran. 2014. "Improved shear design rules for lipped channel beams with  
408 web openings." *J. Constr. Steel Res.*, 97: 127-142. <https://doi.org/10.1016/j.jcsr.2014.01.011>.

409 Keerthan, P., and M. Mahendran. 2015. "Experimental investigation and design of lipped channel  
410 beams in shear." *Thin-Walled Struct.*, 86: 174-184. <https://doi.org/10.1016/j.tws.2014.08.024>

411 LaBoube, R.A, and Yu W.W. 1978. "Strength of cold-formed steel beam webs in bending, shear, and a  
412 combination of bending and shear." Rolla, USA: American Iron and Steel Institute, University of  
413 Missouri-Rolla.

414 Li, H.T., and B. Young. 2019. "Cold-formed high-strength steel tubular structural members under  
415 combined bending and bearing." *J. Struct. Eng.*, 145(8): 04019081. [https://doi.org/](https://doi.org/10.1061/(ASCE)ST.1943-541X.0002371)  
416 10.1061/(ASCE)ST.1943-541X.0002371.

417 Pham, C.H., and G.J. Hancock. 2009. "Shear buckling of thin-walled channel sections." *J. Constr. Steel*  
418 *Res.*, 65: 578-585. <https://doi.org/10.1016/j.jcsr.2016.10.013>.

419 Pham, C.H., and G.J. Hancock. 2010a. "Experimental investigation of high strength C-sections in  
420 combined bending and shear." *J. Struct. Eng.*, 136: 866-878.  
421 [https://doi.org/10.1061/\(ASCE\)ST.1943-541X.0000172](https://doi.org/10.1061/(ASCE)ST.1943-541X.0000172).

422 Pham, C.H., and G.J. Hancock. 2010b. "Numerical simulation of high strength cold-formed purlins in  
423 combined bending and shear." *J. Constr. Steel Res.*, 66: 1205-1217.  
424 <https://doi.org/10.1016/j.jcsr.2010.04.014>

425 Pham, C.H., and G.J. Hancock. 2012. "Direct strength design of cold-formed C-sections for shear and  
426 combined actions." *J Struct Eng*, 138: 759-768. [https://doi.org/10.1061/\(ASCE\)ST.1943-](https://doi.org/10.1061/(ASCE)ST.1943-541X.0000510)  
427 541X.0000510.

428 Pham, S. H., C. H. Pham, and G. J. Hancock. 2017a. "Direct strength method of design for channel  
429 sections in shear with square and circular web holes," *J. Struct. Eng.*, 143(6): 04017017.  
430 [https://doi.org/10.1061/\(ASCE\)ST.1943-541X.0001765](https://doi.org/10.1061/(ASCE)ST.1943-541X.0001765).

431 Pham, C.H. 2017b. "Shear buckling of plates and thin-walled channel sections with holes." *J. Constr.*  
432 *Steel Res.*, 128: 800-811. <https://doi.org/10.1016/j.jcsr.2016.10.013>.

433 Pham, S.H, C.H. Pham, C.A. Rogers, and G.J. Hancock. 2020a. "Shear strength experiments and design  
434 of cold-formed steel channels with web holes." *J. Struct. Eng.*, 146(1): 04019173.  
435 [https://doi.org/10.1061/\(ASCE\)ST.1943-541X.0002464](https://doi.org/10.1061/(ASCE)ST.1943-541X.0002464).

436 Pham, C.H., and G. J. Hancock. 2020b. "Shear tests and design of cold-formed steel channels with  
437 central square holes." *Thin-Walled Struct.* 149: 106650.  
438 <https://doi.org/10.1016/j.tws.2020.106650>.

439 Pham, D.K, C.H. Pham, S.H. Pham and G. J. Hancock. 2020c. "Experimental investigation of high  
440 strength cold-formed channel sections in shear with rectangular and slotted web openings." *J.*  
441 *Constr. Steel Res.*, 165:105889. <https://doi.org/10.1016/j.jcsr.2019.105889>.

442 Pham, D.K, C.H. Pham and G. J. Hancock. 2020d. "Parametric study for shear design of cold-formed  
443 channels with elongated web openings." *J. Constr. Steel Res.*, 172: 106222.  
444 <https://doi.org/10.1016/j.jcsr.2020.106222>.

445 Roy ,K., H.H. Lau, T.C.H. Ting, B. Chen, and J.B.P. Lim. 2020. "Flexural capacity of gapped built-up cold-  
446 formed steel channel sections including web stiffeners" *J. Constr. Steel Res.*, 172: 106154.  
447 <https://doi.org/10.1016/j.jcsr.2020.106154>.

448 Shan, M.Y., R.A. LaBoube, J.E. Langan, and W.W. Yu. 1997. "Cold-formed steel webs with openings:  
449 summary report." *Thin-Walled Struct.*, 27: 79-84. [https://doi.org/10.1016/0263-8231\(96\)00021-3](https://doi.org/10.1016/0263-8231(96)00021-3)

450 Uzzaman, A, J.B.P. Lim, D. Nash, and B. Young. 2017. "Effects of edge-stiffened circular web openings  
451 on the web crippling strength of cold-formed steel channel beams under one-flange loading  
452 conditions." *Eng. Struct.*, 139: 96-107. <https://doi.org/10.1016/j.engstruct.2017.02.042>.

453 Uzzaman, A, J.B.P. Lim, D. Nash, and K. Roy. 2020a. "Cold-formed steel channel beams under end-two-  
454 flange loading condition: Design for edge-stiffened holes, unstiffened holes and plain webs." *Thin-  
455 Walled Struct.*, 147: 106532. <https://doi.org/10.1016/j.tws.2019.106532>.

456 Uzzaman, A, J.B.P. Lim, D. Nash, and K. Roy. 2020b. "Web crippling behaviour of cold-formed steel  
457 channel sections with edge-stiffened and unstiffened circular holes under interior-two-flange  
458 loading condition." *Thin-Walled Struct.*, 154: 106813. <https://doi.org/10.1016/j.tws.2020.106813>.

459 Yu, C. 2012. "Cold-formed steel flexural member with edge stiffened web openings: behavior,  
460 optimization, and design." *J. Constr. Steel Res.*, 71: 210-218.  
461 <https://doi.org/10.1016/j.jcsr.2011.09.008>.

## Nomenclature

$a$	Shear span;
$b_f$	Width of flange;
$b_l$	Width of lip;
COV	Coefficient of variation;
CFS	Cold-formed steel;
$d_1$	Clear height of web;
$d_{wh}$	Diameter of web hole;
$E$	Young's modulus of elasticity;
FEA	Finite element analysis;
$f_y$	Yield strength;
$L$	Total length of test specimen;
LVDTs	Linear variable displacement transducers;
$q$	Length of stiffener;
$q_s$	Reduction factor;
$q_{s(AISI\&AS/NZS)}$	Reduction factor predicted from AISI (2016) and AS/NZS (2018)
$q_{s(Shan)}$	Reduction factor predicted from design rules proposed by Shan et al. (1997)
$q_{s(KM)}$	Reduction factor predicted from design rules proposed by Keerthan and Mahendran et al. (2013b, 2014);
$r_i$	Inside corner radius of section;
$t_w$	Thickness of web;
$V_{DSM-1}$	Shear capacity predicted from the DSM design rules in shear without TFA;
$V_{DSM-2}$	Shear capacity predicted from the DSM design rules in shear with TFA;
$V_{EXP}$	Shear capacity predicted from laboratory tests;
$V_{EXP-1.0}$	Experimental shear capacity of specimens with aspect ratios of 1.0;
$V_{EXP-1.5}$	Experimental shear capacity of specimens with aspect ratios of 1.5;
$V_{FEA}$	Shear capacity predicted from finite element (FEA);
$V_{KM}$	Shear capacity predicted from the design equations proposed by Keerthan and Mahendran et al. (2015);
$\sigma_{0.2}$	Static 0.2% proof stress;
$\sigma_u$	Static ultimate tensile strength;
$\sigma_{true}$	True stress ;
$\epsilon_{true(pl)}$	True strain ;

**Table 1. Measured dimensions and shear capacity for specimens with flanges restrained by straps**

a) Section 240

Specimen	Web height	Total length	Web thickness	Stiffener length	Hole diameter	Aspect ratio	Ratio	Ratio	Shear capacity obtained from test	Reduction factor
	$d_1$	$L$	$t_w$	$q$	$d_{wh}$	$a/d_1$	$d_1/t_w$	$d_{wh}/d_1$	$V_{EXP}$	$q_s$
	(mm)	(mm)	(mm)	(mm)	(mm)				(kN)	
<b>Plain section</b>										
240-A1.0-D0-NH-FR	239.3	672.6	1.81	-	-	1.0	132.2	-	53.7	1.00
240-A1.5-D0-NH-FR	239.3	908.9	1.81	-	-	1.5	132.2	-	37.5	1.00
<b>Edge-stiffened holes</b>										
240-A1.0-D140-EH-FR	236.5	672.6	1.86	13	148.5	1.0	127.2	0.63	35.3	0.66
240-A1.5-D140-EH-FR	238.3	908.9	1.86	13	147.5	1.5	128.1	0.62	31.2	0.83
240-A1.0-D90-EH-FR	239.3	672.6	1.85	13	98.0	1.0	129.4	0.41	49.1	0.91
240-A1.5-D90-EH-FR	238.5	908.9	1.85	13	97.5	1.5	128.9	0.41	37.5	1.00
<b>Un-stiffened holes</b>										
240-A1.0-D140-UH-FR	235.5	672.6	1.86	-	149.5	1.0	126.6	0.63	30.4	0.56
240-A1.5-D140-UH-FR	235.1	908.9	1.85	-	148.2	1.5	127.1	0.63	24.9	0.66
240-A1.0-D90-UH-FR	235.5	672.6	1.88	-	98.0	1.0	125.3	0.42	45.3	0.84
240-A1.5-D90-UH-FR	235.5	908.9	1.88	-	98.5	1.5	125.3	0.42	33.4	0.89

b) Section 290

Specimen	Web height	Total length	Web thickness	Stiffener length	Hole diameter	Aspect ratio	Ratio	Ratio	Shear capacity obtained from test	Reduction factor
	$d_1$	$L$	$t_w$	$q$	$d_{wh}$	$a/d_1$	$d_1/t_w$	$d_{wh}/d_1$	$V_{EXP}$	$q_s$
	(mm)	(mm)	(mm)	(mm)	(mm)				(kN)	
<b>Plain section</b>										
290-A1.0-D0-NH-FR	289.6	771.2	2.10	-	-	1.0	137.9	-	73.1	1.00
290-A1.5-D0-NH-FR	285.6	1056.	2.11	-	-	1.5	135.4	-	49.1	1.00
<b>Edge-stiffened holes</b>										
290-A1.0-D140-EH-FR	287.6	771.2	2.15	13	148.3	1.0	133.8	0.52	55.9	0.76
290-A1.5-D140-EH-FR	288.5	1056.	2.13	13	147.5	1.5	135.4	0.51	50.0	0.92
290-A1.0-D90-EH-FR	285.6	771.2	2.16	13	98.5	1.0	132.2	0.34	64.8	0.88
290-A1.5-D90-EH-FR	287.0	1056.	2.16	13	99.0	1.5	132.9	0.34	51.3	0.94
<b>Un-stiffened holes</b>										
290-A1.0-D140-UH-FR	285.0	771.2	2.18	-	148.5	1.0	130.7	0.52	51.2	0.70
290-A1.5-D140-UH-FR	286.5	1056.	2.17	-	149.5	1.5	132.0	0.52	42.1	0.86
290-A1.0-D90-UH-FR	285.0	771.2	2.18	-	99.5	1.0	130.7	0.35	63.9	0.87
290-A1.5-D90-UH-FR	285.6	1056.	2.17	-	99.0	1.5	131.6	0.35	48.1	0.98

**Table 2. Measured dimensions and shear capacity for specimens with flanges unrestrained by straps**

Specimen	Web height	Total length	Web thickness	Stiffener length	Hole diameter	Aspect ratio	Ratio	Ratio	Shear capacity obtained from test	Reduction factor
	$d_1$	$L$	$t_w$	$q$	$d_{wh}$	$a/d_1$	$d_1/t_w$	$d_{wh}/d_1$	$V_{EXP}$	$q_s$
	(mm)	(mm)	(mm)	(mm)	(mm)				(kN)	
<b>Plain section</b>										
240-A1.0-D0-NH-FU	235.3	672.6	1.85	-	-	1.0	127.1	-	46.9	1.00
240-A1.5-D0-NH-FU	236.3	908.9	1.85	-	-	1.5	127.7	-	35.0	1.00
<b>Edge-stiffened holes</b>										
240-A1.0-D140-EH-FU	237.3	672.6	1.86	13	148.9	1.0	127.6	0.63	31.7	0.67
240-A1.5-D140-EH-FU	238.3	908.9	1.85	13	147.5	1.5	128.8	0.62	28.7	0.82
240-A1.0-D90-EH-FU	235.5	672.6	1.87	13	96.5	1.0	125.9	0.41	41.0	0.87
240-A1.5-D90-EH-FU	237.3	908.9	1.85	13	93.5	1.5	128.3	0.39	35.2	1.01
<b>Un-stiffened holes</b>										
240-A1.0-D140-UH-FU	237.3	672.6	1.86	-	148.5	1.0	127.6	0.63	26.0	0.55
240-A1.5-D140-UH-FU	238.0	908.9	1.86	-	147.0	1.5	128.0	0.62	22.8	0.65
240-A1.0-D90-UH-FU	237.5	672.6	1.87	-	98.0	1.0	127.0	0.41	36.0	0.78
240-A1.5-D90-UH-FU	238.9	908.9	1.85	-	97.5	1.5	129.1	0.41	30.7	0.88

**Table 3. Material properties of specimens obtained from tensile coupon tests**

Section	Coupon ID	Thickness	Yield stress	Ultimate stress
		$t_w$ /mm	$\sigma_{0.2}$ /MPa	$\sigma_u$ /MPa
Section 240	240-1	1.81	302.3	372.8
	240-2	1.82	300.9	380.1
	240-3	1.81	301.2	383.9
	Mean	1.81	301.6	378.9
Section 290	290-1	2.11	310.2	383.1
	290-2	2.10	308.6	387.4
	290-3	2.13	306.5	390.6
	Mean	2.11	308.5	387.0

**Table 4. Comparison of shear capacity of specimens with and without flange restraints**

Specimen	Shear capacity predicted from test		Capacity reduction
	With straps	Without straps	
	(kN)	(kN)	(%)
240-A1.0-D0-NH	53.7	46.9	12.6
240-A1.5-D0-NH	37.5	35.0	6.7
240-A1.0-D140-EH	35.3	31.7	10.2
240-A1.5-D140-EH	31.2	28.7	8.0
240-A1.0-D90-EH	49.1	41.0	16.5
240-A1.5-D90-EH	37.5	35.2	6.1
240-A1.0-D140-UH	30.4	26.0	13.3
240-A1.5-D140-UH	24.9	22.8	8.4
240-A1.0-D90-UH	45.3	36.0	20.5
240-A1.5-D90-UH	33.4	30.7	8.1
Mean			11.04

**Table 5. Comparison of shear capacity of specimens having aspect ratios of 1.0 and 1.5**

Specimen	Shear capacity predicted from test		Capacity reduction
	$a/d_1=1.0$	$a/d_1=1.5$	
	$V_{EXP-1.0}$ (kN)	$V_{EXP-1.5}$ (kN)	(%)
240-D0-NH-FR	53.7	37.5	43.2
290-D0-NH-FR	73.1	49.1	48.9
240-D0-NH-FU	46.9	35.0	34.0
240-D140-EH-FR	35.3	31.2	13.1
240-D90-EH-FR	49.1	37.5	30.9
290-D140-EH-FR	55.9	50.0	11.8
290-D90-EH-FR	64.8	51.3	26.3
240-D140-EH-FU	31.7	28.7	10.5
240-D90-EH-FU	41.0	35.2	16.5
240-D140-UH-FR	30.4	24.9	18.1
240-D90-UH-FR	45.3	33.4	35.6
290-D140-UH-FR	51.2	42.1	21.6
290-D90-UH-FR	63.9	48.1	32.8
240-D140-UH-FU	26.0	22.8	14.0
240-D90-UH-FU	36.0	30.7	17.3
Mean			24.9



**Table 6. Comparison of shear capacity obtained from tests and FEA for all test specimens**

Specimen	Aspect	Ratio	Ratio	Shear capacity		Test/FEA
	$a/d_1$	$d_1/t_w$	$d_{wh}/d_1$	Test	FEA	
				(kN)	(kN)	
<b>Plain section</b>						
240-A1.0-D0-NH-FR	1.0	132.2	-	53.7	50.6	1.06
240-A1.5-D0-NH-FR	1.5	132.2	-	37.5	38.3	0.98
240-A1.0-D0-NH-FU	1.0	132.2	-	46.9	49.5	0.95
240-A1.5-D0-NH-FU	1.5	127.7	-	35.0	38.0	0.92
290-A1.0-D0-NH-FR	1.0	137.9	-	73.1	70.7	1.03
290-A1.5-D0-NH-FR	1.5	135.4	-	49.1	53.5	0.92
<b>Edge-stiffened holes</b>						
240-A1.0-D140-EH-FR	1.0	127.2	0.63	35.3	32.1	1.10
240-A1.5-D140-EH-FR	1.5	128.1	0.62	31.2	30.3	1.03
240-A1.0-D90-EH-FR	1.0	129.4	0.41	49.1	46.0	1.07
240-A1.5-D90-EH-FR	1.5	128.9	0.41	37.5	40.1	0.94
240-A1.0-D140-EH-FU	1.0	127.6	0.63	31.7	31.3	1.01
240-A1.5-D140-EH-FU	1.5	128.8	0.62	28.7	29.1	0.99
240-A1.0-D90-EH-FU	1.0	125.9	0.41	41.0	44.4	0.92
240-A1.5-D90-EH-FU	1.5	128.3	0.39	35.2	37.9	0.93
290-A1.0-D140-EH-FR	1.0	133.8	0.52	55.9	51.5	1.09
290-A1.5-D140-EH-FR	1.5	135.4	0.51	50.0	44.9	1.11
290-A1.0-D90-EH-FR	1.0	132.2	0.34	64.8	68.2	0.95
290-A1.5-D90-EH-FR	1.5	132.9	0.34	51.3	55.3	0.93
<b>Un-stiffened holes</b>						
240-A1.0-D140-UH-FR	1.0	126.6	0.63	30.4	28.3	1.07
240-A1.5-D140-UH-FR	1.5	127.1	0.63	24.9	22.7	1.10
240-A1.0-D90-UH-FR	1.0	125.3	0.42	45.3	43.1	1.05
240-A1.5-D90-UH-FR	1.5	125.3	0.42	33.4	34.0	0.98
240-A1.0-D140-UH-FU	1.0	127.6	0.63	26.0	24.0	1.08
240-A1.5-D140-UH-FU	1.5	128.0	0.62	22.8	21.4	1.07
240-A1.0-D90-UH-FU	1.0	127.0	0.41	36.0	38.3	0.94
240-A1.5-D90-UH-FU	1.5	129.1	0.41	30.7	32.0	0.96
290-A1.0-D140-UH-FR	1.0	130.7	0.52	51.2	43.2	1.18
290-A1.5-D140-UH-FR	1.5	132.0	0.52	42.1	38.0	1.11
290-A1.0-D90-UH-FR	1.0	130.7	0.35	63.9	63.9	1.00
290-A1.5-D90-UH-FR	1.5	131.6	0.35	48.1	51.9	0.93
Mean						1.01
COV						0.07

**Table 7. Shear capacity predicted from the parametric study for varying thickness, hole diameter ratio and stiffener length ratio (aspect ratio=1.0)**

(a) Section 240

Thickness	Hole ratio	Shear capacity obtained from the parametric study, $V_{FEA}$ (kN)						
$t_w$ (mm)	$A (d_{wh}/d_1)$	Without hole	With un-stiffened hole	With edge-stiffened hole				
				Q0.04	Q0.06	Q0.08	Q0.10	Q0.12
1.0	0.1	22.1	22.0	22.3	22.6	22.8	23.1	23.6
1.0	0.3	22.1	17.8	19.1	19.4	19.9	20.1	20.4
1.0	0.5	22.1	11.7	14.2	14.6	15.3	15.9	16.2
1.0	0.7	22.1	6.6	9.4	9.7	10.2	11.1	11.8
1.5	0.1	40.4	38.1	40.2	40.6	41.0	41.8	42.8
1.5	0.3	40.4	32.4	35.5	35.8	36.1	37.1	37.9
1.5	0.5	40.4	21.0	27.0	28.0	29.0	29.7	30.5
1.5	0.7	40.4	12.1	18.0	18.7	19.7	20.2	20.9
2.0	0.1	56.5	56.4	56.9	57.3	58.0	58.3	58.8
2.0	0.3	56.5	48.3	49.1	49.9	50.6	51.5	52.5
2.0	0.5	56.5	32.2	39.7	40.7	41.9	42.6	43.5
2.0	0.7	56.5	19.6	25.4	26.3	27.4	28.6	29.5
2.5	0.1	86.1	85.6	86.9	87.7	88.6	89.4	90.4
2.5	0.3	86.1	69.2	73.1	74.4	75.9	77.2	78.8
2.5	0.5	86.1	45.5	54.4	56.1	57.7	59.3	60.8
2.5	0.7	86.1	27.0	36.7	38.3	39.6	41.1	42.7

(a) Section 290

Thickness	Hole ratio	Shear capacity obtained from the parametric study, $V_{FEA}$ (kN)						
$t_w$ (mm)	$A (d_{wh}/d_1)$	Without hole	With un-stiffened hole	With edge-stiffened hole				
				Q0.04	Q0.06	Q0.08	Q0.10	Q0.12
1.0	0.1	25.1	24.7	25.5	25.7	26.1	26.6	26.8
1.0	0.3	25.1	20.7	22.5	22.7	23.2	23.7	24.0
1.0	0.5	25.1	14.6	17.2	17.6	18.0	18.6	19.0
1.0	0.7	25.1	9.1	11.1	11.7	12.4	13.3	13.8
1.5	0.1	46.2	44.7	46.8	47.2	47.7	48.3	48.9
1.5	0.3	46.2	37.4	42.0	42.5	43.2	43.8	44.6
1.5	0.5	46.2	24.9	29.5	30.9	32.3	33.7	35.1
1.5	0.7	46.2	15.1	20.3	21.5	22.8	24.1	25.5
2.0	0.1	66.5	66.0	67.3	68.0	68.8	69.6	70.5
2.0	0.3	66.5	56.7	60.8	61.6	62.6	63.5	64.5
2.0	0.5	66.5	37.4	45.5	47.2	48.7	50.3	52.1
2.0	0.7	66.5	22.7	29.5	31.5	33.3	35.5	37.5
2.5	0.1	90.5	89.7	91.5	92.5	93.3	94.5	95.5
2.5	0.3	90.5	74.0	82.0	83.2	84.2	85.3	86.5
2.5	0.5	90.5	52.1	61.1	63.2	65.1	66.8	68.9
2.5	0.7	90.5	32.3	39.2	41.6	43.7	46.2	48.5

**Table 8. Comparison of shear capacity obtained from tests, parametric study and current design formulae for CFS plain channels (aspect ratio=1.0)**

Specimen	Thickness	Ratio	Shear capacity (kN)				Comparison		
	$t_w$ (mm)	$d_1/t_w$	$V_{EXP\&FEA}$	$V_{DSM-1}$	$V_{DSM-2}$	$V_{KM}$	$V_{EXP\&FEA}/V_{DSM-1}$	$V_{EXP\&FEA}/V_{DSM-2}$	$V_{EXP\&FEA}/V_{KM}$
<b>Experiments</b>									
240-D0-NH-FR	1.81	132.2	53.7	42.7	54.3	49.8	1.26	0.99	1.08
290-D0-NH-FR	2.10	137.9	73.1	55.1	75.0	66.6	1.33	0.97	1.10
<b>Parametric study</b>									
240-D0-NH-T1.0	1.0	238.0	22.1	7.2	19.6	14.4	3.07	1.13	1.53
240-D0-NH-T1.5	1.5	158.0	40.4	24.3	39.4	32.4	1.66	1.03	1.25
240-D0-NH-T2.0	2.0	118.0	56.5	57.6	64.2	63.4	0.98	0.88	0.89
240-D0-NH-T2.5	2.5	94.0	86.1	89.1	93.3	93.7	0.97	0.92	0.92
290-D0-NH-T1.0	1.0	288.0	25.1	5.9	20.9	15.5	4.25	1.20	1.62
290-D0-NH-T1.5	1.5	191.3	46.2	20.1	42.2	32.1	2.30	1.09	1.44
290-D0-NH-T2.0	2.0	143.0	66.5	47.6	69.1	59.5	1.40	0.96	1.12
290-D0-NH-T2.5	2.5	114.0	90.5	92.9	100.8	99.6	0.98	0.90	0.91
Mean							1.82	1.01	1.18
COV							0.56	0.10	0.21

**Table 9. Comparison of shear capacity reduction factor obtained from tests, parametric study and current design formulae for CFS channels with un-stiffened web holes (aspect ratio=1.0)**

Specimen	Ratio	Shear capacity reduction factor ( $q_s$ )				Comparison		
	$d_{wh}/d_1$	$q_s$	$q_{s(AISI\&AS/NZS)}$	$q_{s(Shan)}$	$q_{s(KM)}$	$q_s/q_{s(AISI\&AS/NZS)}$	$q_s/q_{s(Shan)}$	$q_s/q_{s(KM)}$
<b>Experiments</b>								
240-D140-UH-FR	0.63	0.56	0.64	0.22	0.39	0.88	2.54	1.43
240-D90-UH-FR	0.42	0.84	0.81	0.30	0.66	1.04	2.80	1.25
290-D140-UH-FR	0.52	0.70	0.76	0.26	0.53	0.92	2.29	1.34
290-D90-UH-FR	0.35	0.87	0.91	0.45	0.76	0.96	1.93	1.14
<b>Parametric study</b>								
240-D24-UH-T1.0	0.1	1.00	NA	1.00	0.94	NA	1.00	1.06
240-D72-UH-T1.0	0.3	0.81	NA	0.61	0.81	NA	1.32	1.00
240-D120-UH-T1.0	0.5	0.53	NA	0.27	0.55	NA	1.96	0.96
240-D168-UH-T1.0	0.7	0.30	NA	0.19	0.29	NA	1.57	1.03
290-D29-UH-T1.0	0.1	1.00	NA	1.00	0.94	NA	1.00	1.06
290-D87-UH-T1.0	0.3	0.82	NA	0.61	0.82	NA	1.35	1.01
290-D145-UH-T1.0	0.5	0.58	NA	0.27	0.56	NA	2.15	1.04
290-D203-UH-T1.0	0.7	0.36	NA	0.19	0.29	NA	1.91	1.25
240-D24-UH-T1.5	0.1	0.94	1.00	1.00	0.94	0.94	0.94	1.00
240-D72-UH-T1.5	0.3	0.80	1.00	0.61	0.81	0.80	1.31	0.99
240-D120-UH-T1.5	0.5	0.52	0.94	0.27	0.55	0.55	1.93	0.95
240-D168-UH-T1.5	0.7	0.30	NA	0.19	0.29	NA	1.58	1.03
290-D29-UH-T1.5	0.1	0.97	1.00	1.00	0.94	0.97	0.97	1.03
290-D87-UH-T1.5	0.3	0.81	1.00	0.61	0.82	0.81	1.32	1.00
290-D145-UH-T1.5	0.5	0.54	1.00	0.27	0.56	0.54	2.00	0.96
290-D203-UH-T1.5	0.7	0.33	NA	0.19	0.29	NA	1.72	1.14
240-D24-UH-T2.0	0.1	1.00	1.00	1.00	0.94	1.00	1.00	1.06
240-D72-UH-T2.0	0.3	0.86	0.85	0.61	0.81	1.01	1.41	1.06
240-D120-UH-T2.0	0.5	0.57	0.69	0.27	0.55	0.81	2.07	1.02
240-D168-UH-T2.0	0.7	0.35	NA	0.19	0.29	NA	1.79	1.17
290-D29-UH-T2.0	0.1	1.00	1.00	1.00	0.94	1.00	1.00	1.06
290-D87-UH-T2.0	0.3	0.86	1.00	0.61	0.82	0.86	1.41	1.05
290-D145-UH-T2.0	0.5	0.56	0.84	0.27	0.56	0.67	2.07	1.00
290-D203-UH-T2.0	0.7	0.34	NA	0.19	0.29	NA	1.79	1.17
240-D24-UH-T2.5	0.1	0.99	0.81	1.00	0.94	1.22	1.00	1.06
240-D72-UH-T2.5	0.3	0.80	0.68	0.61	0.81	1.18	1.31	0.99
240-D120-UH-T2.5	0.5	0.53	0.55	0.27	0.55	0.96	1.96	0.96
240-D168-UH-T2.5	0.7	0.31	NA	0.19	0.29	NA	1.63	1.07
290-D29-UH-T2.5	0.1	0.99	0.98	1.00	0.94	1.01	0.99	1.06
290-D87-UH-T2.5	0.3	0.82	0.82	0.61	0.82	1.00	1.34	1.00
290-D145-UH-T2.5	0.5	0.58	0.67	0.27	0.56	0.85	2.11	1.02
290-D203-UH-T2.5	0.7	0.36	NA	0.19	0.29	NA	1.89	1.24
Mean						0.91	1.62	1.07
COV						0.18	0.29	0.10

NA:  $h/t_w$  ratio or  $d_{wh}$  exceeds the limit of AS/NZS (2018)

**Table 10. Comparison of shear capacity reduction factor obtained from tests, parametric study, current design formulae and proposed design formulae for channels with edge-stiffened web holes (aspect ratio=1.0)**

Specimen	Ratio	Shear capacity reduction factor ( $q_s$ )					Comparison			
	$d_{wh}/d_1$	$q_s$	$q_{s(AISI\&AS/NZS)}$	$q_{s(Shan)}$	$q_{s(KM)}$	$q_{s(pr)}$	$q_s/q_{s(AISI\&AS/NZS)}$	$q_s/q_{s(Shan)}$	$q_s/q_{s(KM)}$	$q_s/q_{s(pr)}$
<b>Experiments</b>										
240-D140-EH	0.63	0.66	0.64	0.22	0.39	0.59	1.03	3.00	1.69	1.12
240-D90-EH	0.41	0.91	0.81	0.30	0.66	0.83	1.12	3.03	1.38	1.10
290-D140-EH	0.52	0.76	0.76	0.26	0.53	0.79	1.00	2.92	1.43	0.96
290-D90-EH	0.34	0.88	0.91	0.45	0.76	0.93	0.97	1.96	1.16	0.95
<b>Parametric study</b>										
240-D24-EH-T1.5-Q0.04	0.1	1.00	1.00	1.00	0.94	1.01	1.00	1.00	1.06	0.99
240-D72-EH-T1.5-Q0.04	0.3	0.88	1.00	0.61	0.81	0.89	0.88	1.44	1.09	0.99
240-D120-EH-T1.5-Q0.04	0.5	0.67	0.94	0.27	0.55	0.67	0.71	2.48	1.22	1.00
240-D168-EH-T1.5-Q0.04	0.7	0.45	NA	0.19	0.29	0.43	NA	2.37	1.55	1.05
240-D24-EH-T1.5-Q0.06	0.1	1.00	1.00	1.00	0.94	1.02	1.00	1.00	1.06	0.98

240-D72-EH-T1.5-Q0.06	0.3	0.89	1.00	0.61	0.81	0.90	0.89	1.46	1.10	0.99
240-D120-EH-T1.5-Q0.06	0.5	0.69	0.94	0.27	0.55	0.69	0.73	2.56	1.25	1.00
240-D168-EH-T1.5-Q0.06	0.7	0.46	NA	0.19	0.29	0.45	NA	2.42	1.59	1.02
240-D24-EH-T2.0-Q0.04	0.1	1.01	1.00	1.00	0.94	1.01	1.01	1.01	1.07	1.00
240-D72-EH-T2.0-Q0.04	0.3	0.87	0.85	0.61	0.81	0.89	1.02	1.43	1.07	0.98
240-D120-EH-T2.0-Q0.04	0.5	0.70	0.79	0.27	0.55	0.67	0.89	2.59	1.27	1.04
240-D168-EH-T2.0-Q0.04	0.7	0.45	NA	0.19	0.29	0.43	NA	2.37	1.55	1.05
240-D24-EH-T2.0-Q0.06	0.1	1.01	1.00	1.00	0.94	1.02	1.01	1.01	1.07	0.99
240-D72-EH-T2.0-Q0.06	0.3	0.88	0.85	0.61	0.81	0.90	1.04	1.44	1.09	0.98
240-D120-EH-T2.0-Q0.06	0.5	0.72	0.79	0.27	0.55	0.69	0.91	2.67	1.31	1.04
240-D168-EH-T2.0-Q0.06	0.7	0.47	NA	0.19	0.29	0.45	NA	2.47	1.62	1.04
290-D29-EH-T1.5-Q0.04	0.1	1.01	1.00	1.00	0.94	1.01	1.01	1.01	1.07	1.00
290-D87-EH-T1.5-Q0.04	0.3	0.91	1.00	0.61	0.81	0.89	0.91	1.49	1.12	1.02
290-D145-EH-T1.5-Q0.04	0.5	0.64	1.00	0.27	0.55	0.67	0.64	2.37	1.16	0.96
290-D203-EH-T1.5-Q0.04	0.7	0.44	NA	0.19	0.29	0.43	NA	2.32	1.52	1.02
290-D29-EH-T1.5-Q0.06	0.1	1.02	1.00	1.00	0.94	1.02	1.02	1.02	1.09	1.00
290-D87-EH-T1.5-Q0.06	0.3	0.92	1.00	0.61	0.81	0.90	0.92	1.51	1.14	1.02
290-D145-EH-T1.5-Q0.06	0.5	0.67	1.00	0.27	0.55	0.69	0.67	2.48	1.22	0.97
290-D203-EH-T1.5-Q0.06	0.7	0.47	NA	0.19	0.29	0.45	NA	2.47	1.62	1.04
290-D29-EH-T2.0-Q0.04	0.1	1.01	1.00	1.00	0.94	1.01	1.01	1.01	1.07	1.00
290-D87-EH-T2.0-Q0.04	0.3	0.91	1.00	0.61	0.81	0.89	0.91	1.49	1.12	1.02
290-D145-EH-T2.0-Q0.04	0.5	0.68	0.84	0.27	0.55	0.67	0.81	2.52	1.24	1.01
290-D203-EH-T2.0-Q0.04	0.7	0.44	NA	0.19	0.29	0.43	NA	2.32	1.52	1.02
290-D29-EH-T2.0-Q0.06	0.1	1.02	1.00	1.00	0.94	1.02	1.02	1.02	1.09	1.00
290-D87-EH-T2.0-Q0.06	0.3	0.93	1.00	0.61	0.81	0.90	0.93	1.52	1.15	1.03
290-D145-EH-T2.0-Q0.06	0.5	0.71	0.84	0.27	0.55	0.69	0.85	2.63	1.29	1.03
290-D203-EH-T2.0-Q0.06	0.7	0.47	NA	0.19	0.29	0.45	NA	2.47	1.62	1.04
Mean							0.93	1.95	1.27	1.01
COV							0.13	0.35	0.16	0.03

**Table 11. Statistical parameters for comparison of shear capacity reduction factor obtained from tests and parametric study against the proposed design formulae**

(a)  $0.1 \leq d_{wh}/d_1 \leq 0.3$

Statistical parameters	$q_{s(FEA\&TEST)} / q_{s(pr)} = 1.04 + 0.67 \frac{q}{d_1} - 0.59 \frac{d_{wh}}{d_1}$
Number of data	80
Mean, $P_m$	1.00
Coefficient of variation, COV	0.02
Reliability index, $\beta$	2.84
Resistance factor, $\phi$	0.85

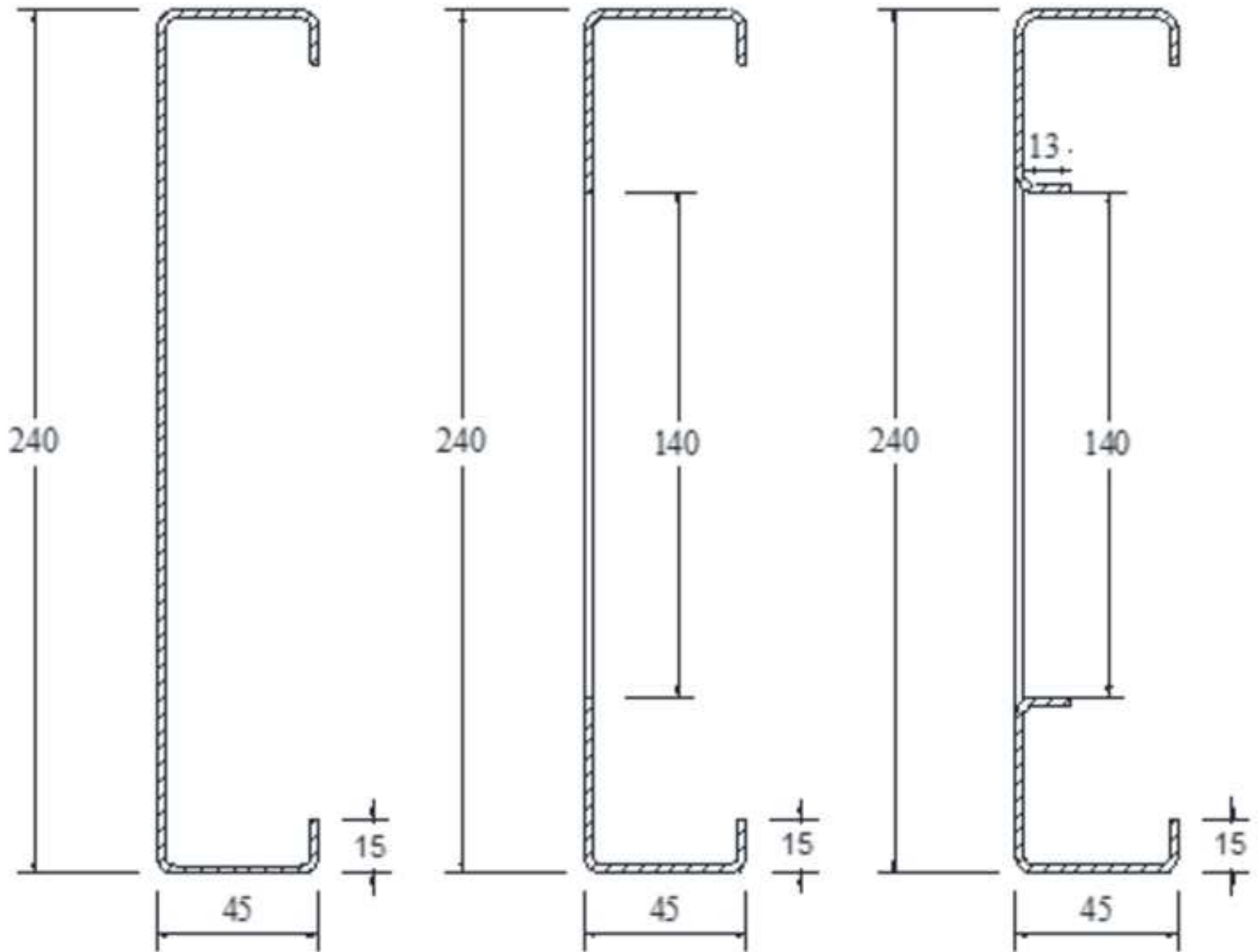
(b)  $0.3 < d_{wh}/d_1 \leq 0.5$

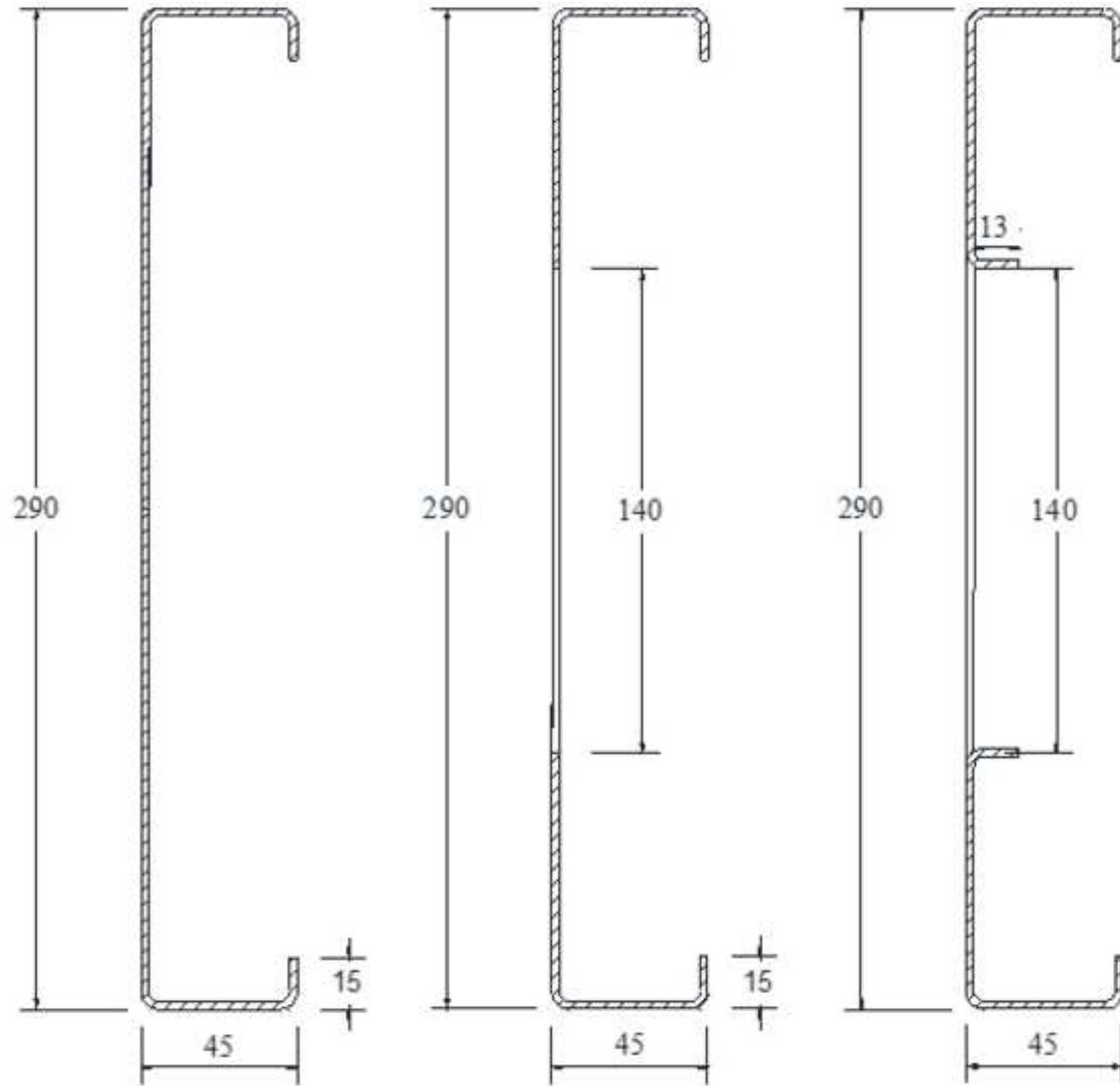
Statistical parameters	$q_{s(FEA\&TEST)} / q_{s(pr)} = 1.42 + 1.08 \frac{q}{d_1} - 1.59 \frac{d_{wh}}{d_1}$
Number of data	42
Mean, $P_m$	1.00
Coefficient of variation, COV	0.04
Reliability index, $\beta$	2.80
Resistance factor, $\phi$	0.85

(c)  $0.5 < d_{wh}/d_1 \leq 0.7$

Statistical parameters	$q_{s(FEA\&TEST)} / q_{s(pr)} = 1.72 + 1.18 \frac{q}{d_1} - 1.91 \frac{d_{wh}}{d_1}$
Number of data	42
Mean, $P_m$	1.00
Coefficient of variation, COV	0.04
Reliability index, $\beta$	2.80
Resistance factor, $\phi$	0.85







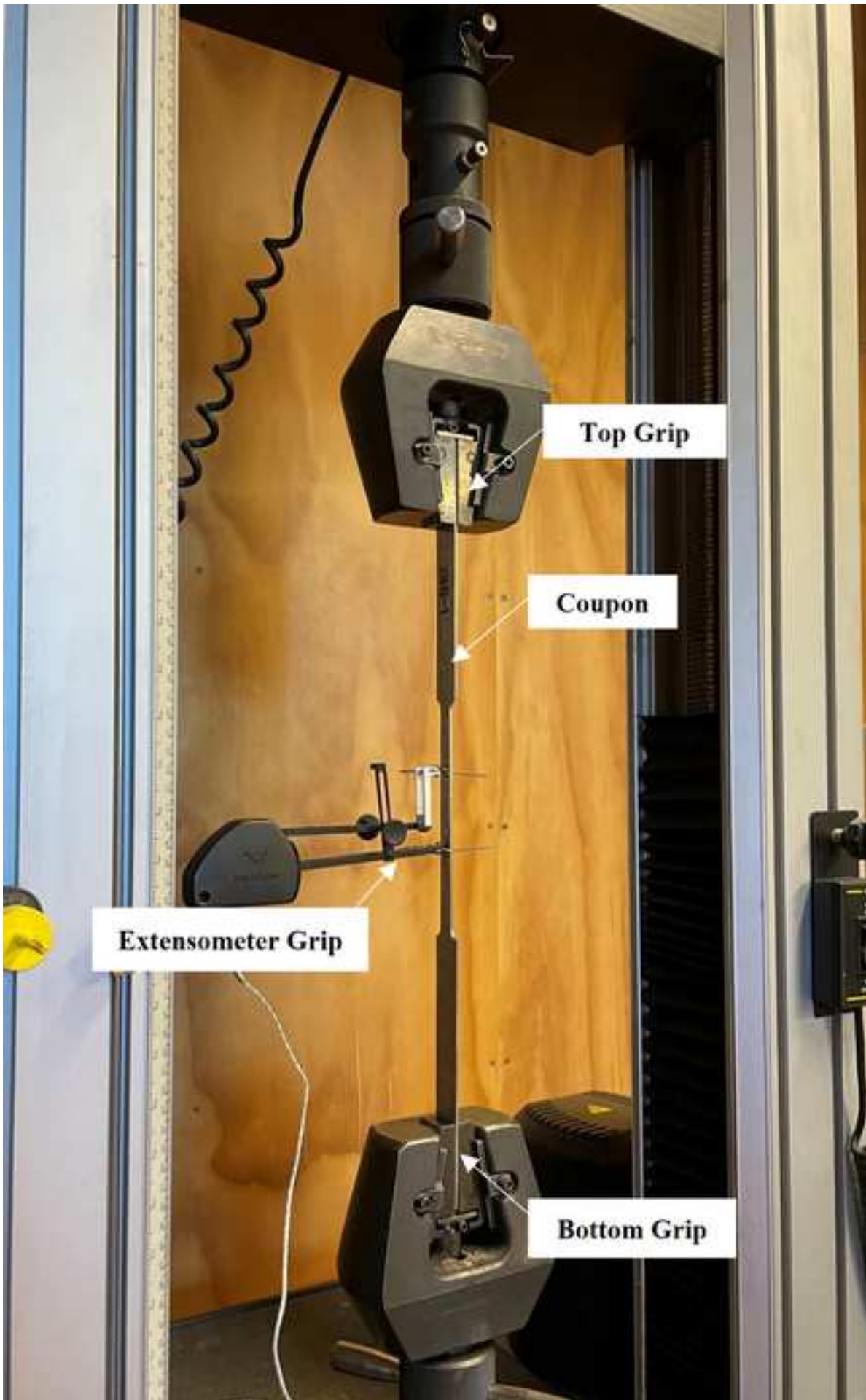


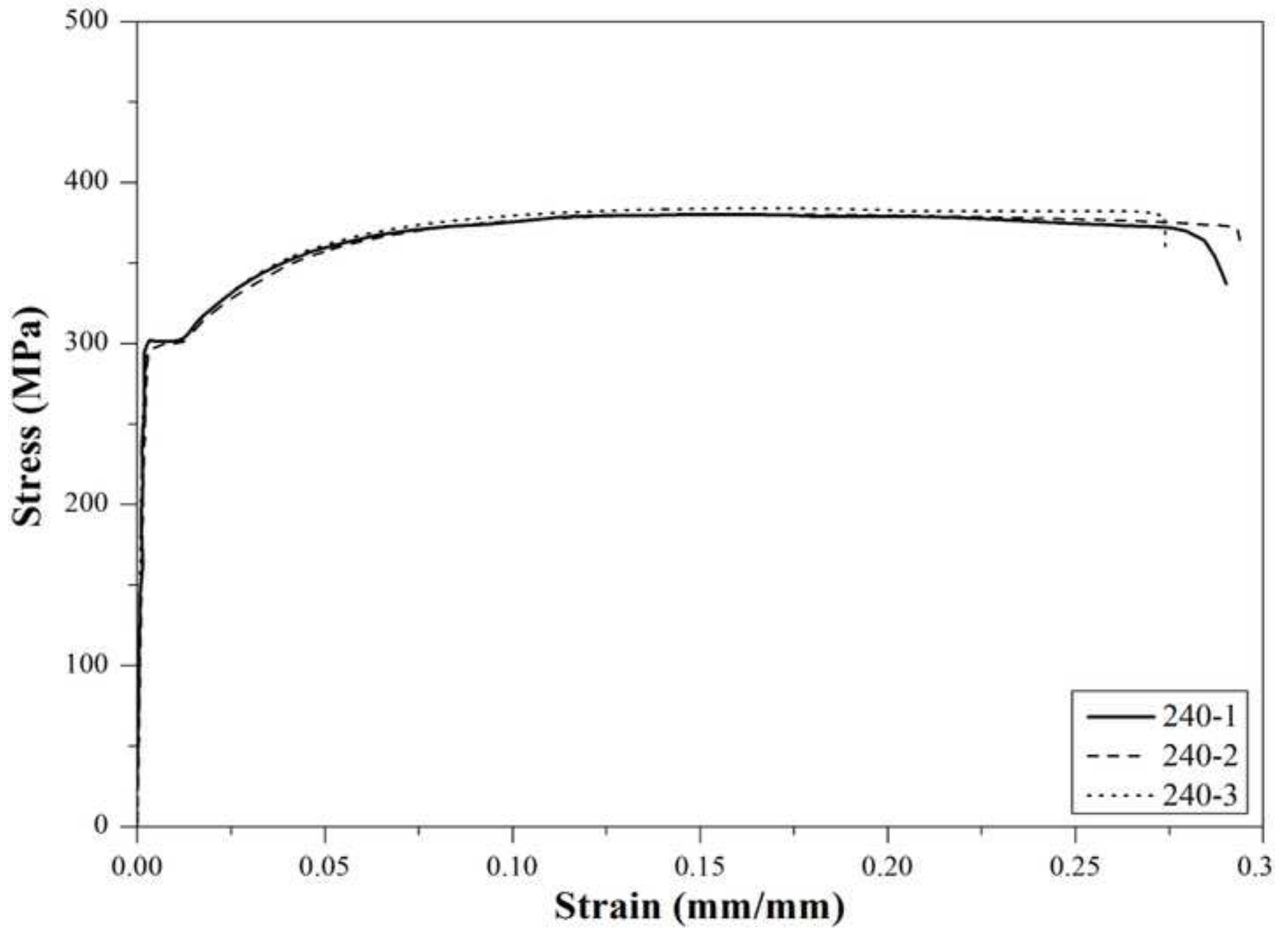


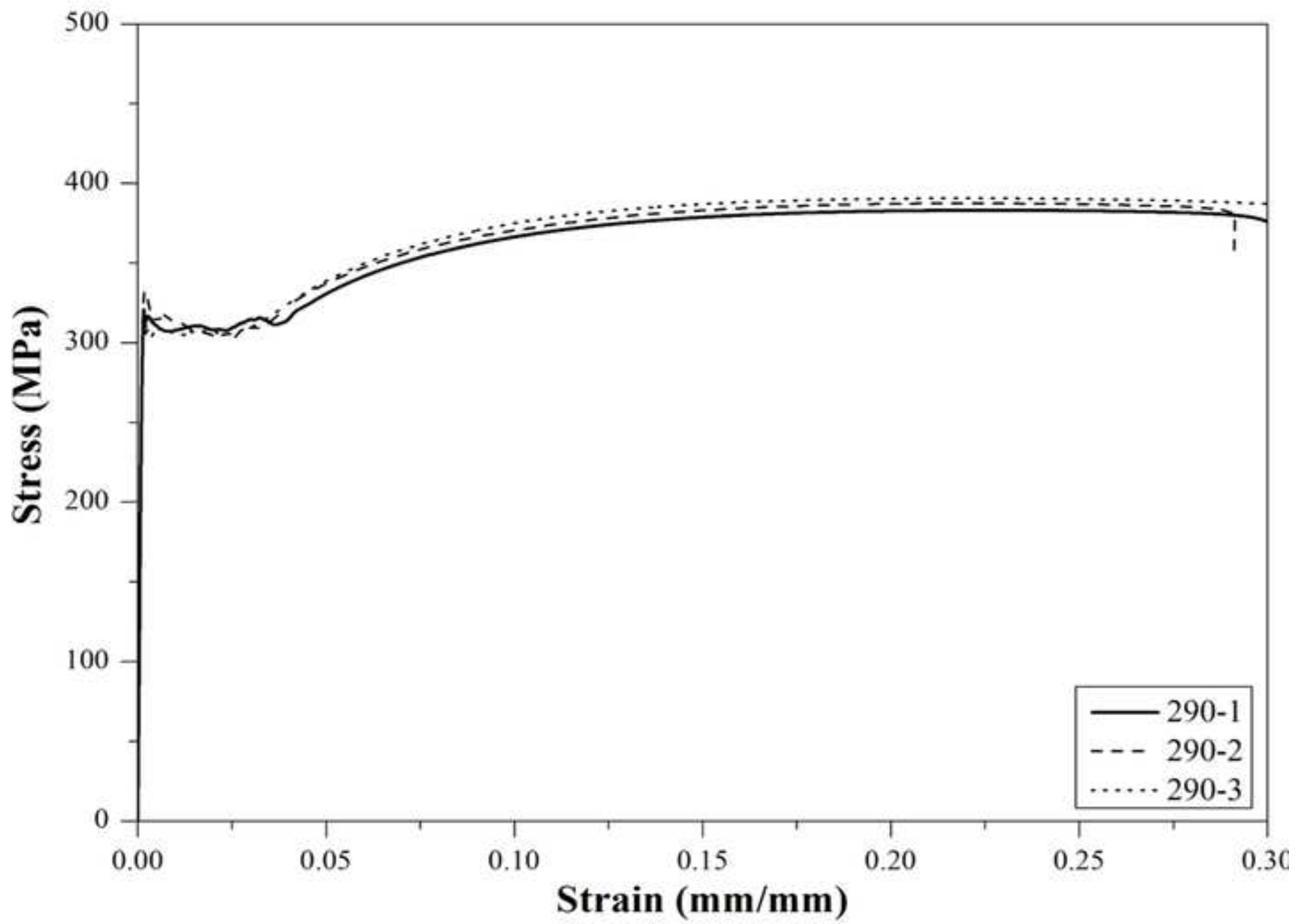




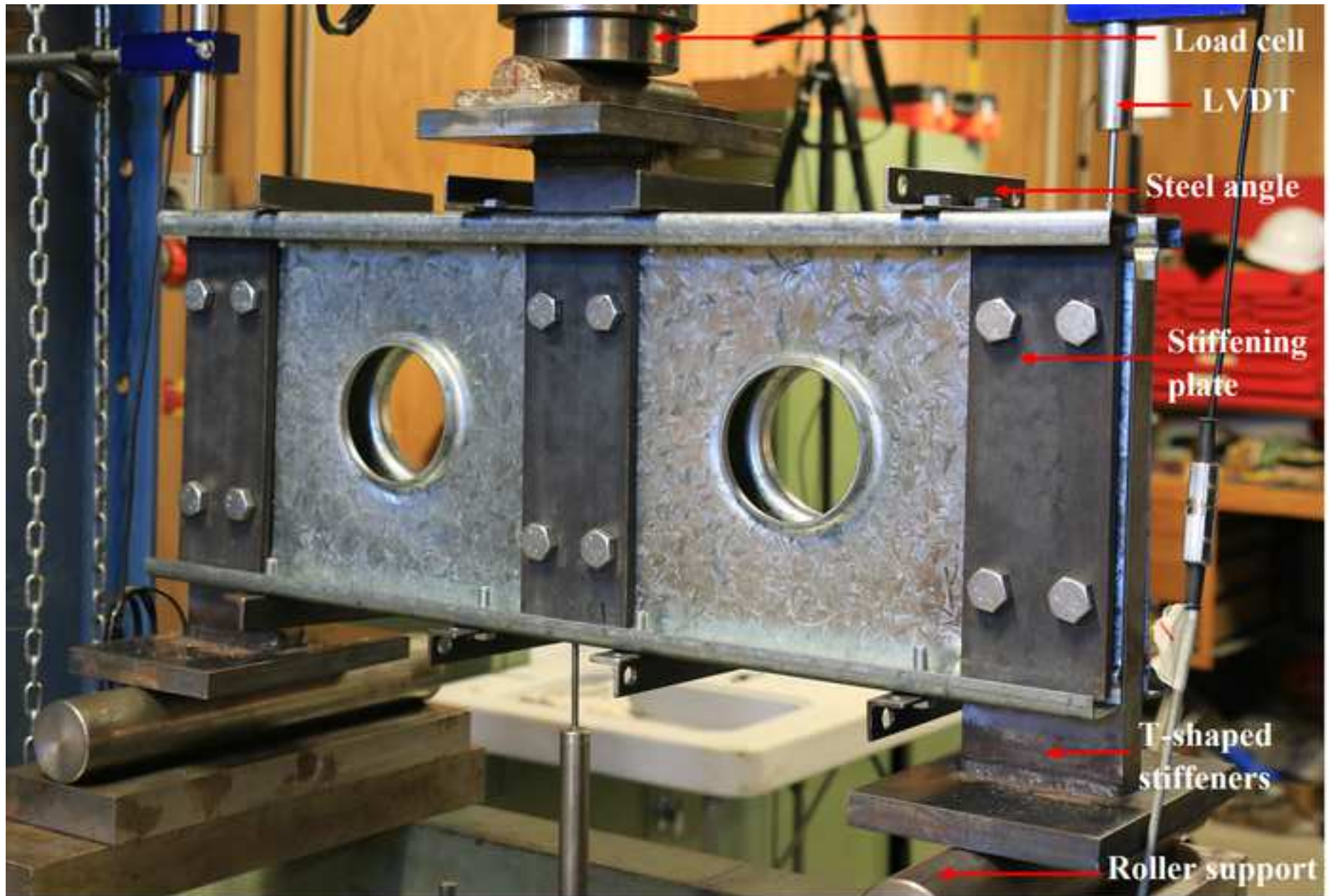


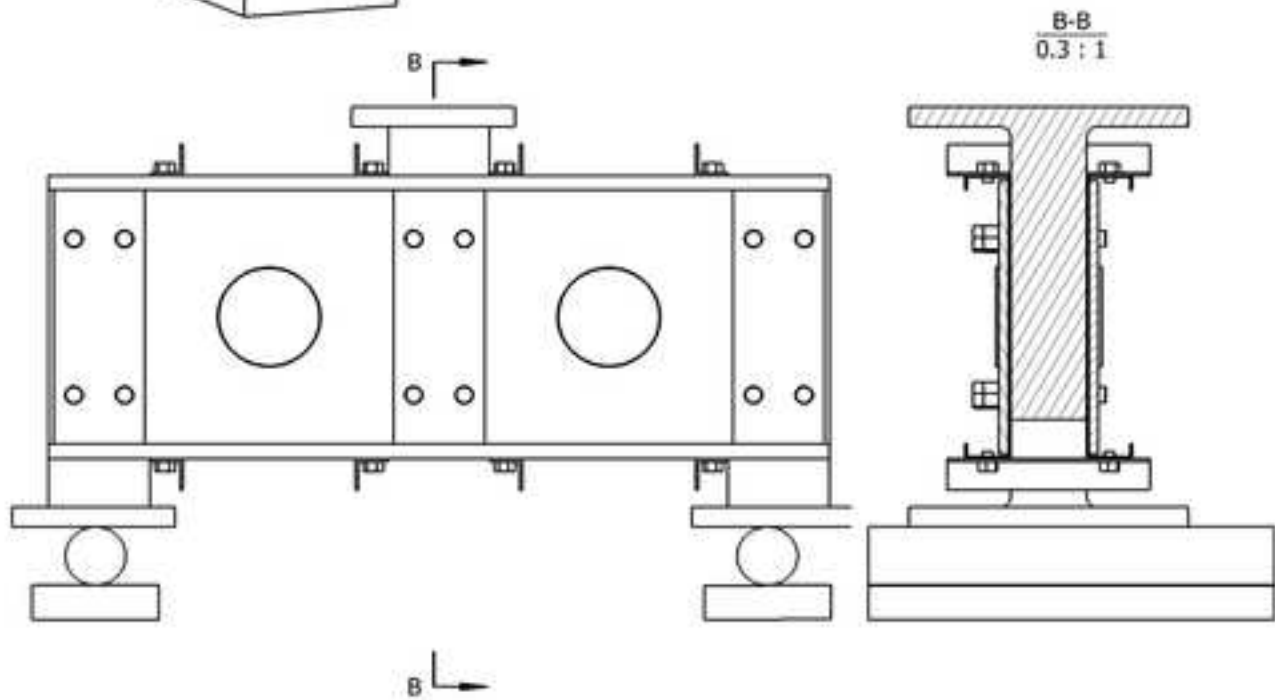
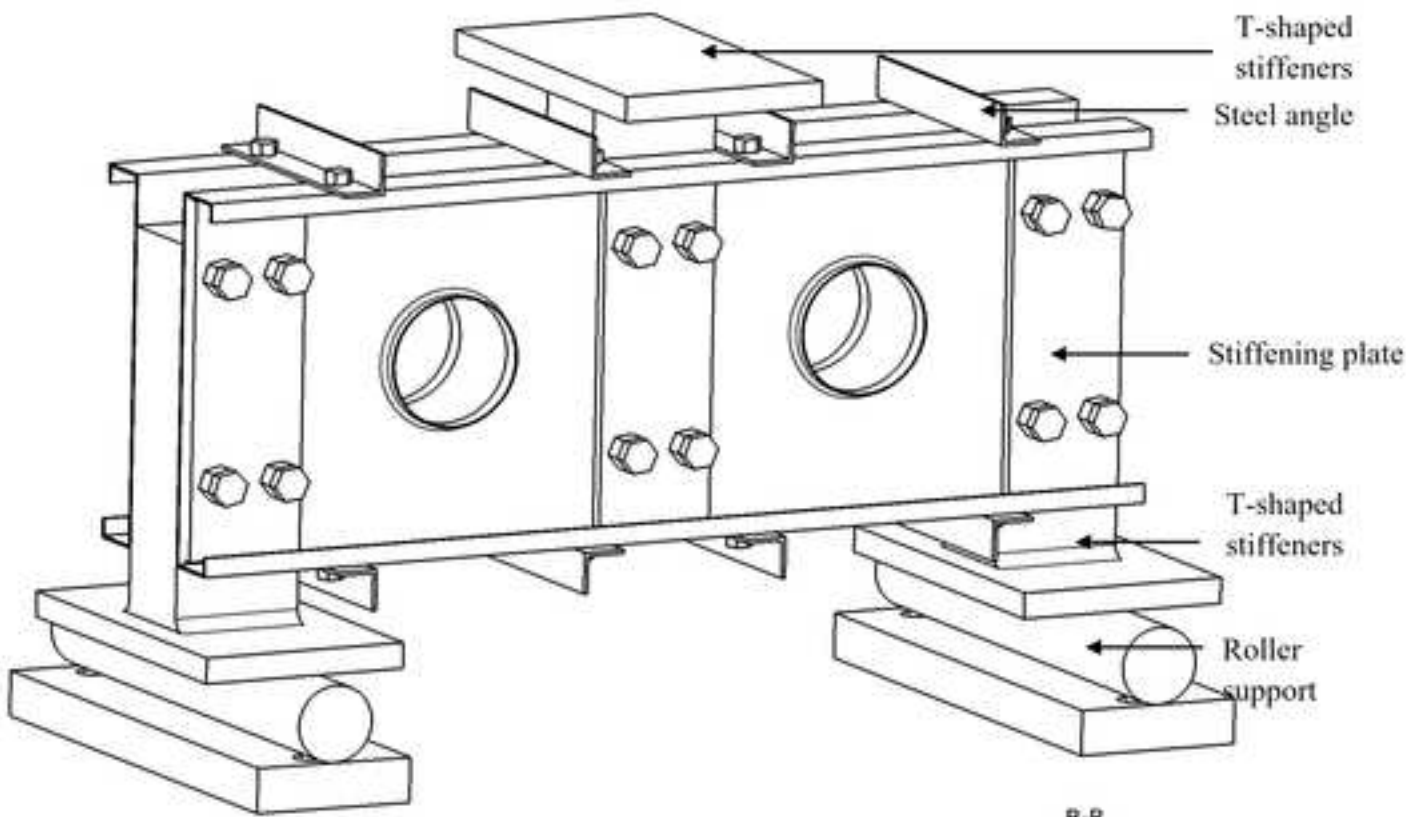


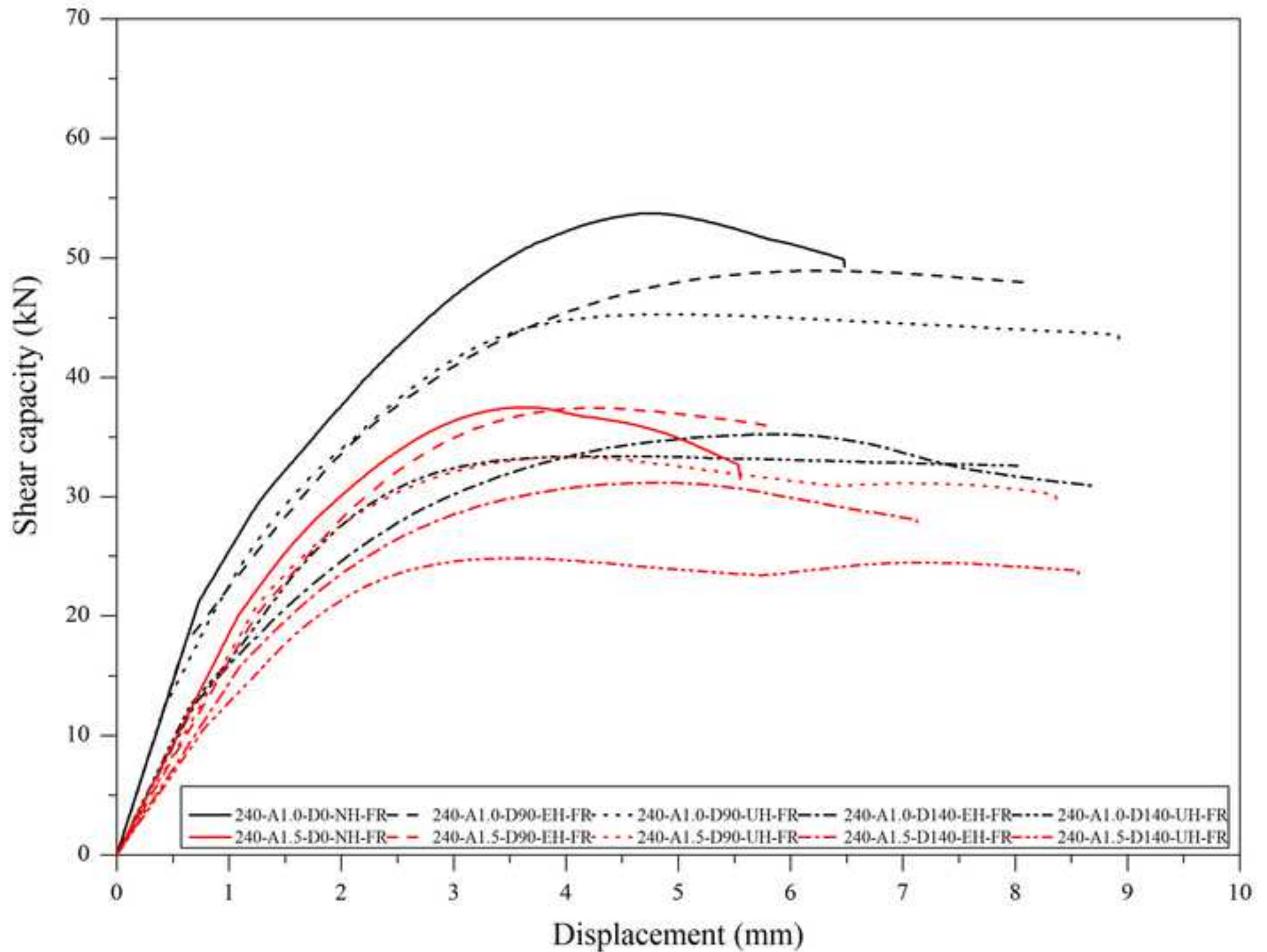




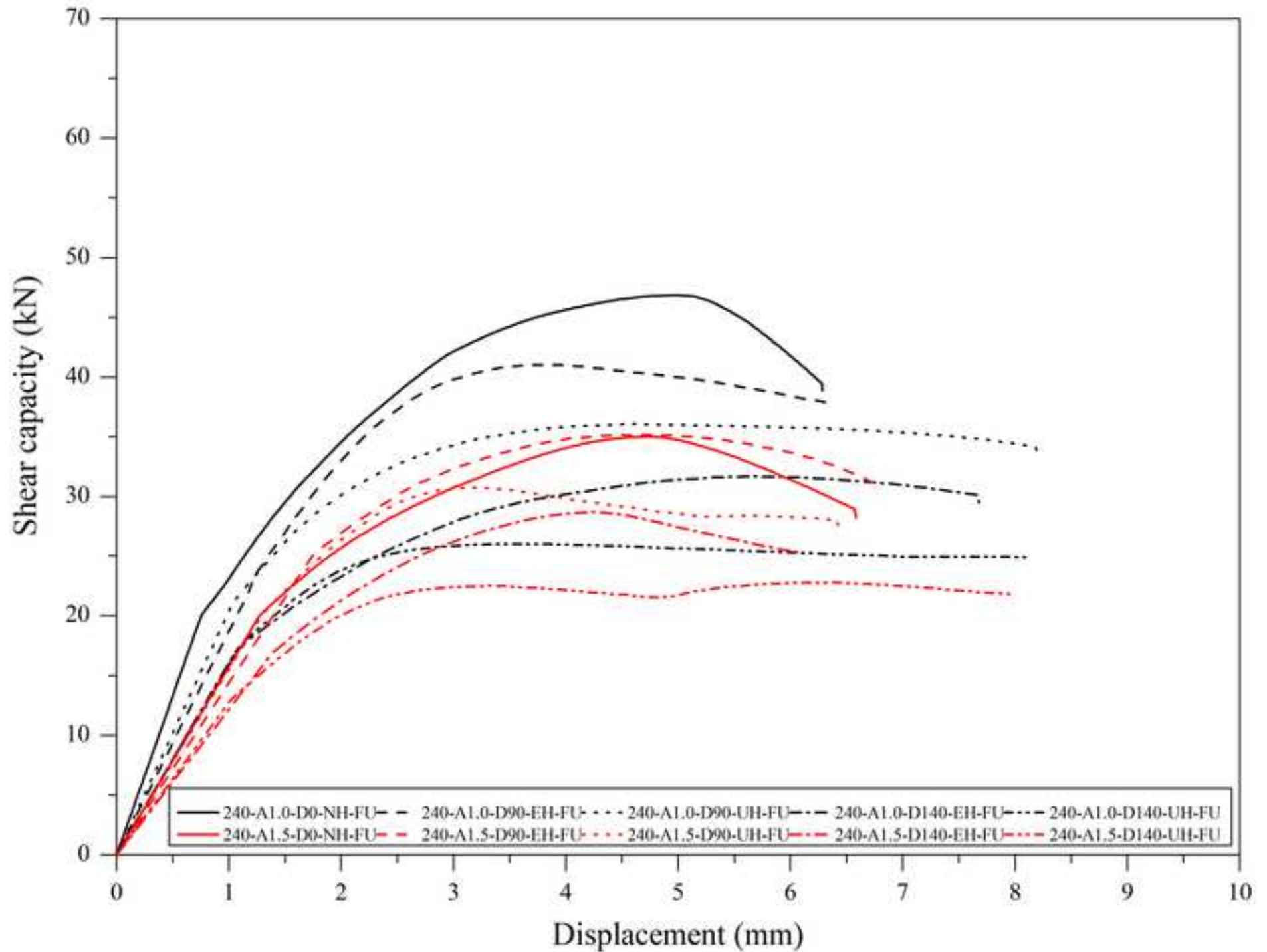


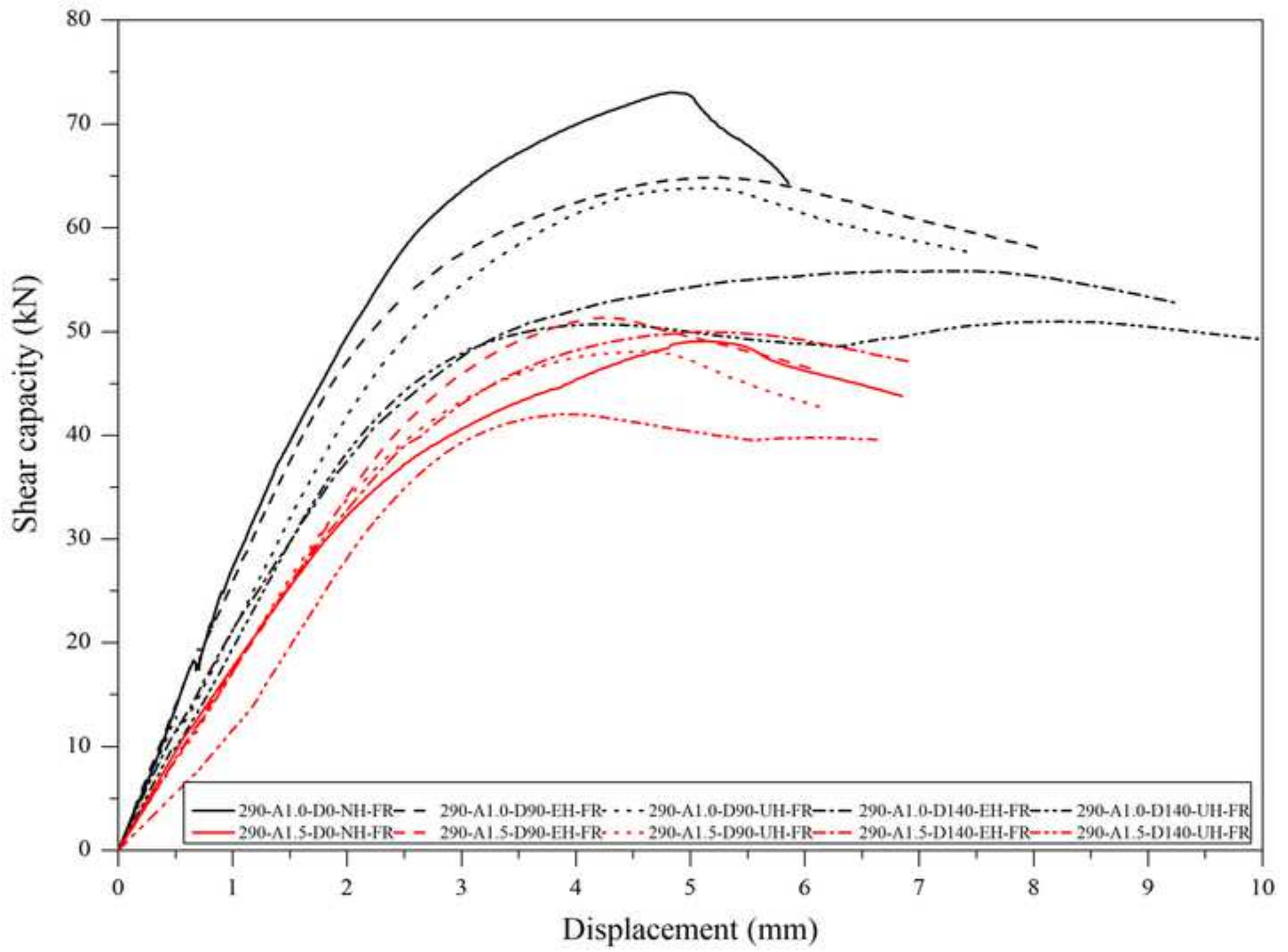


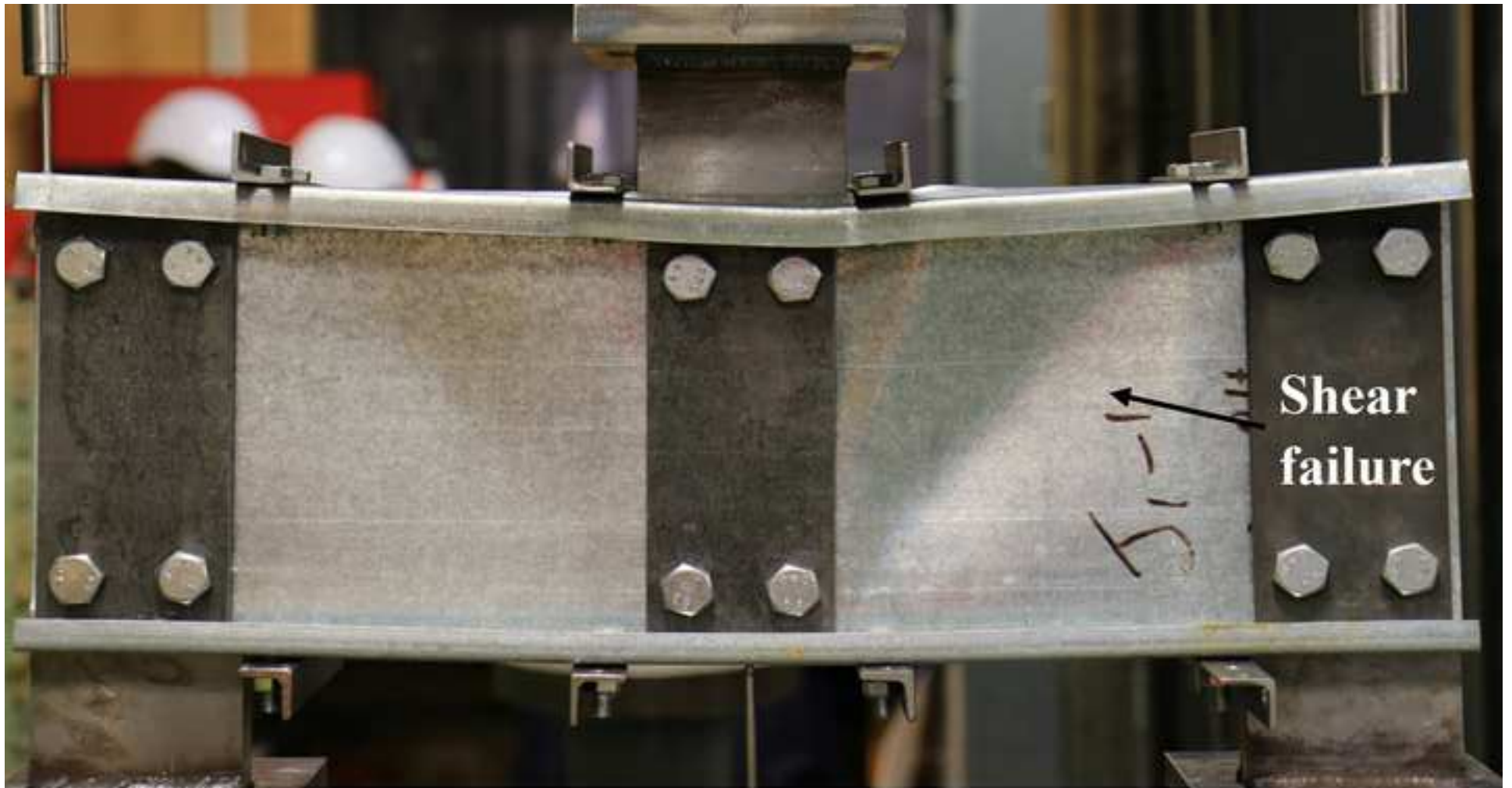






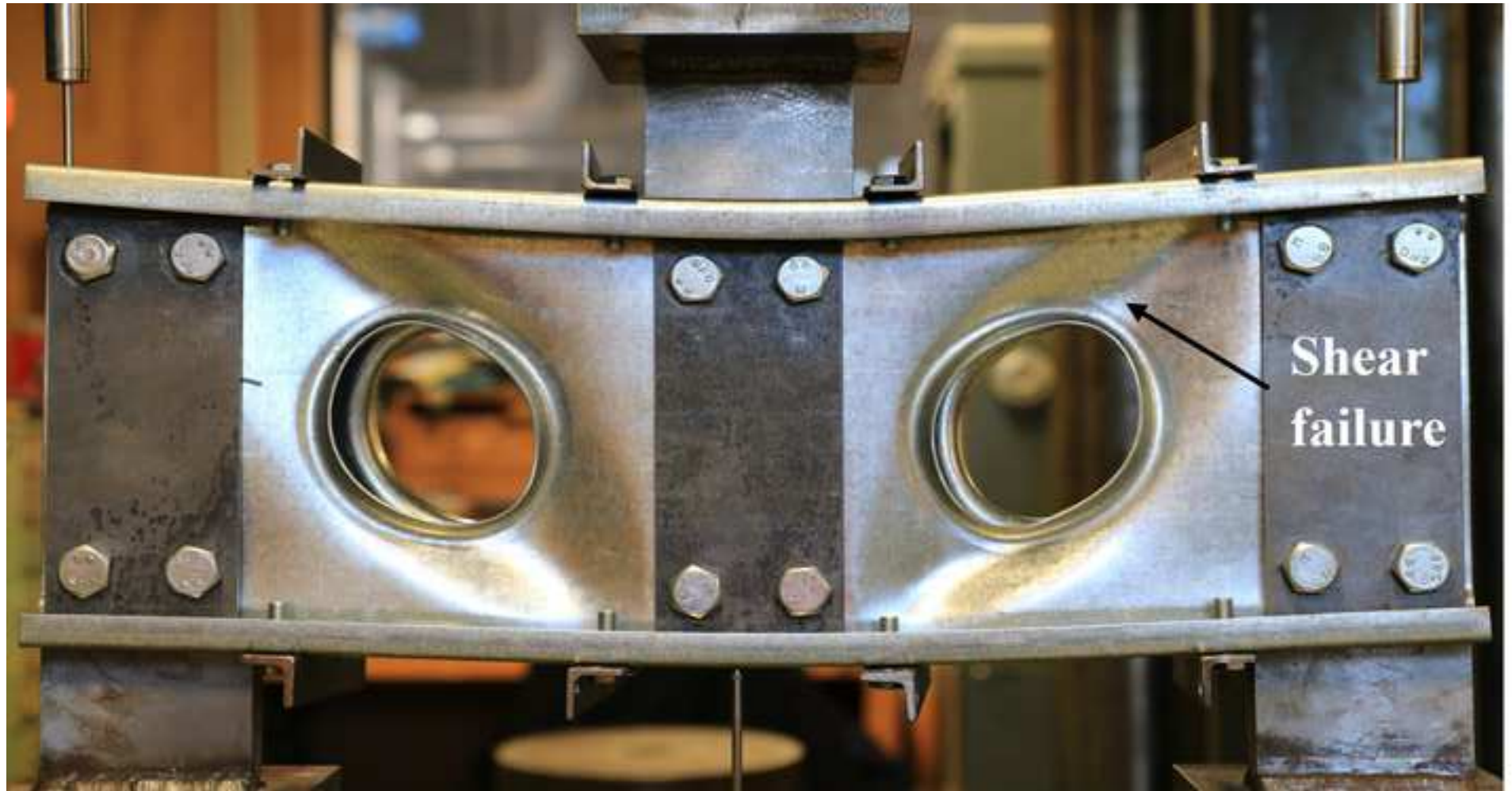


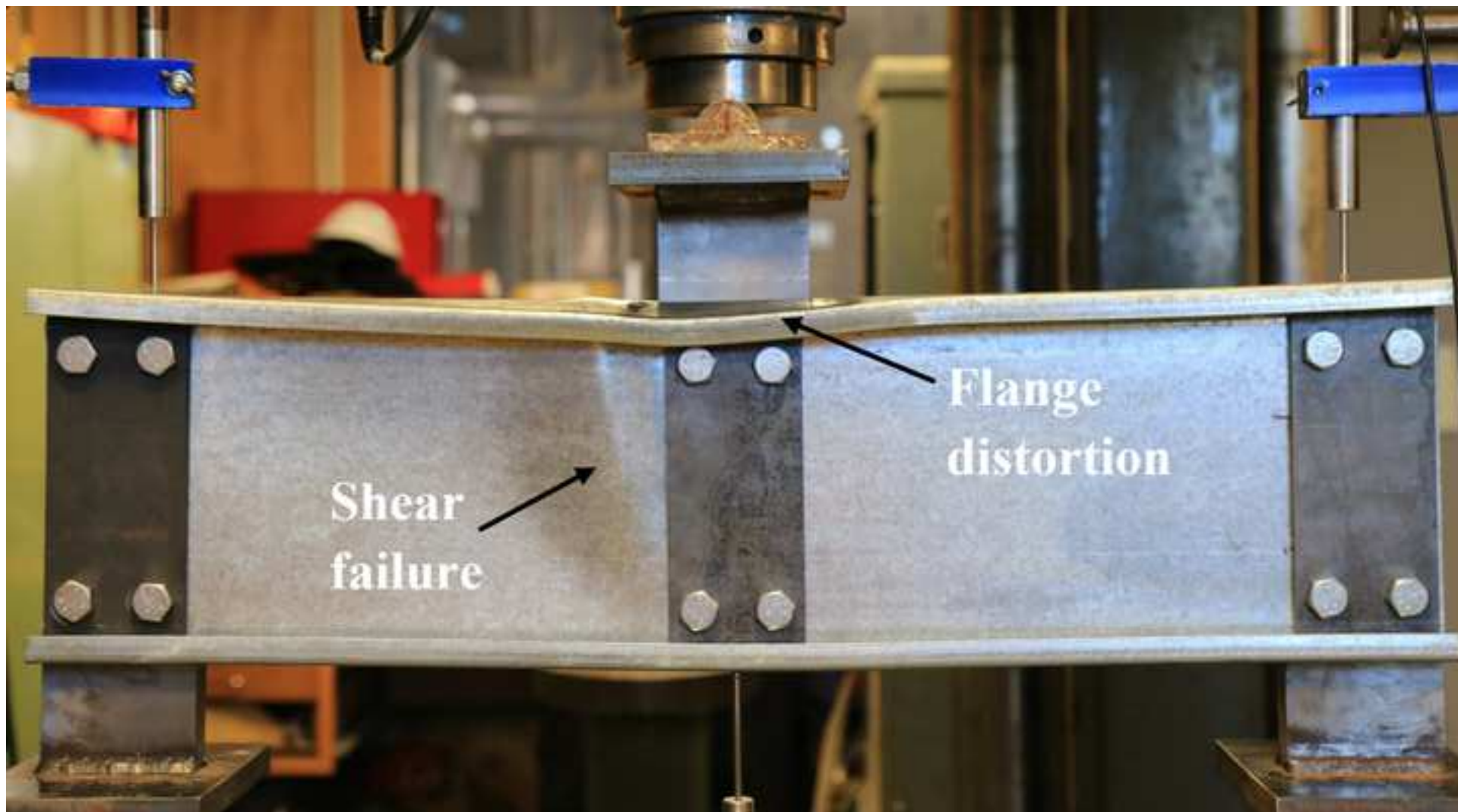








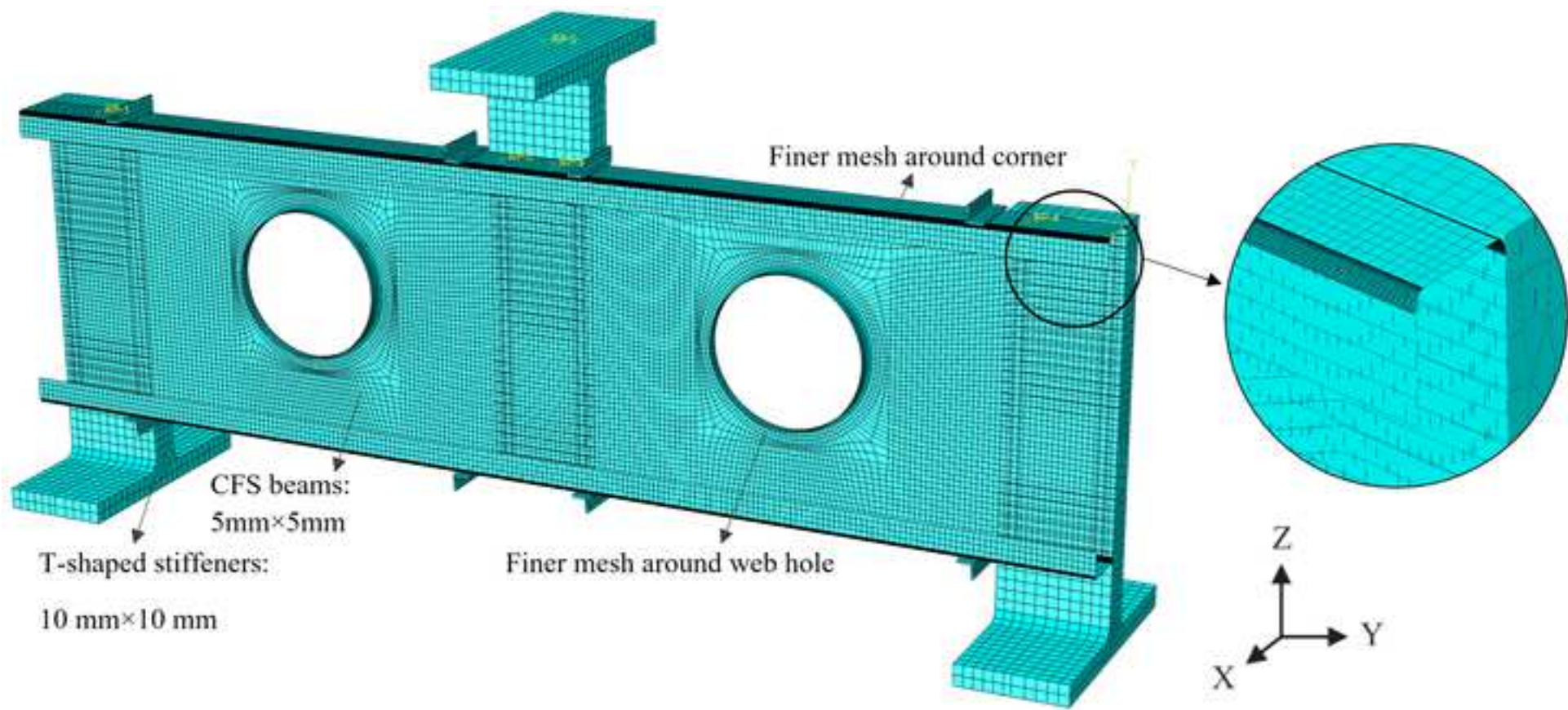


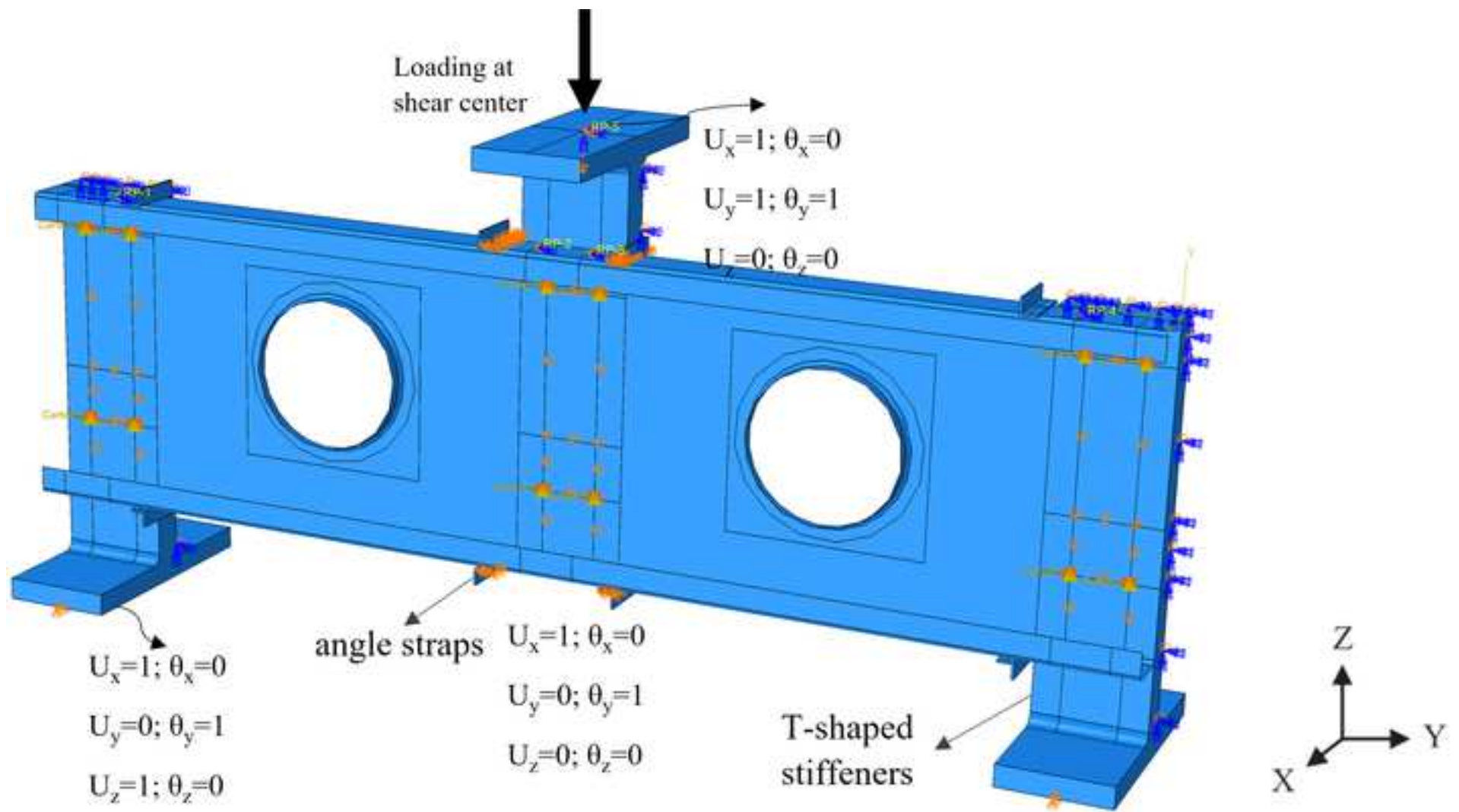


Shear failure

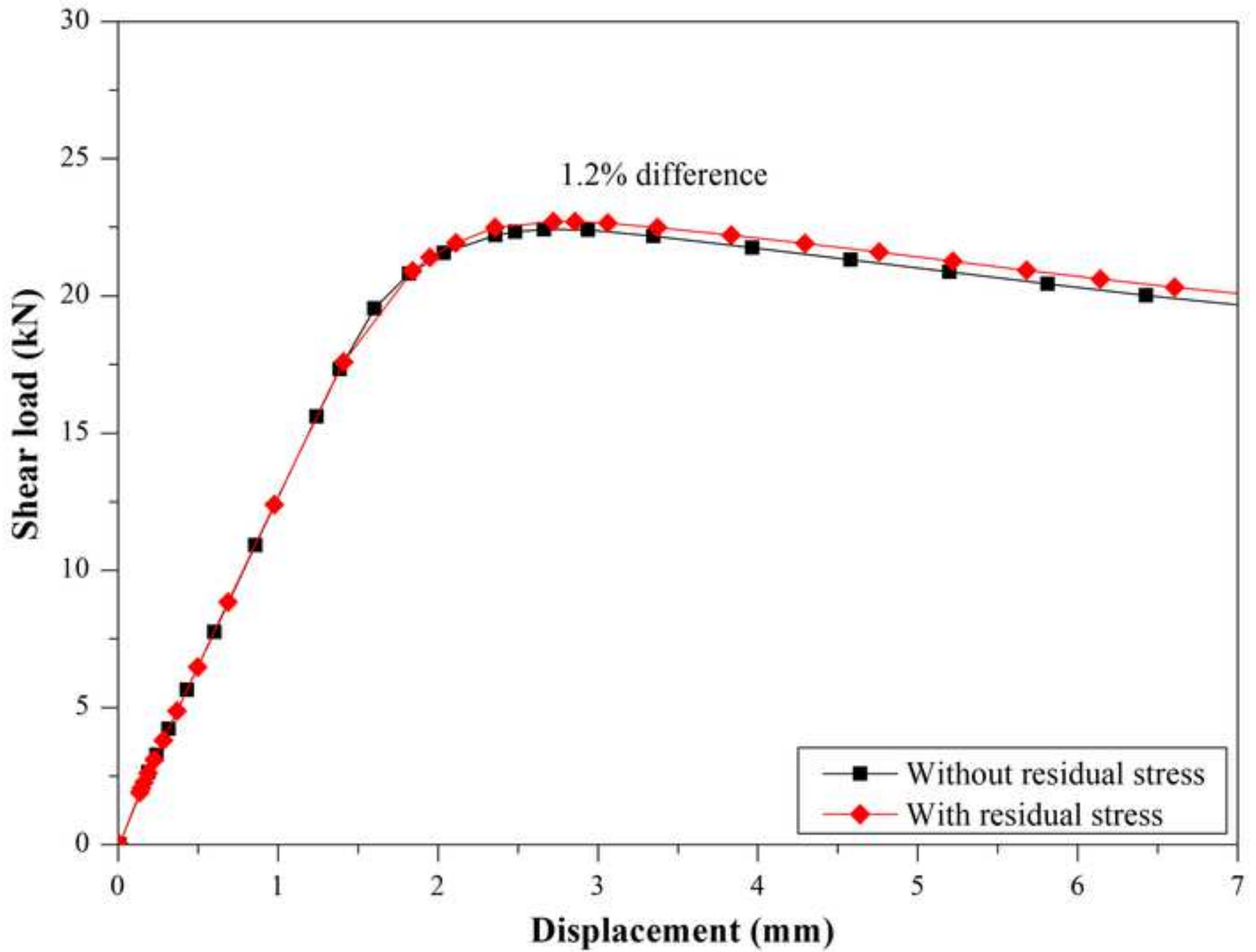
Flange distortion

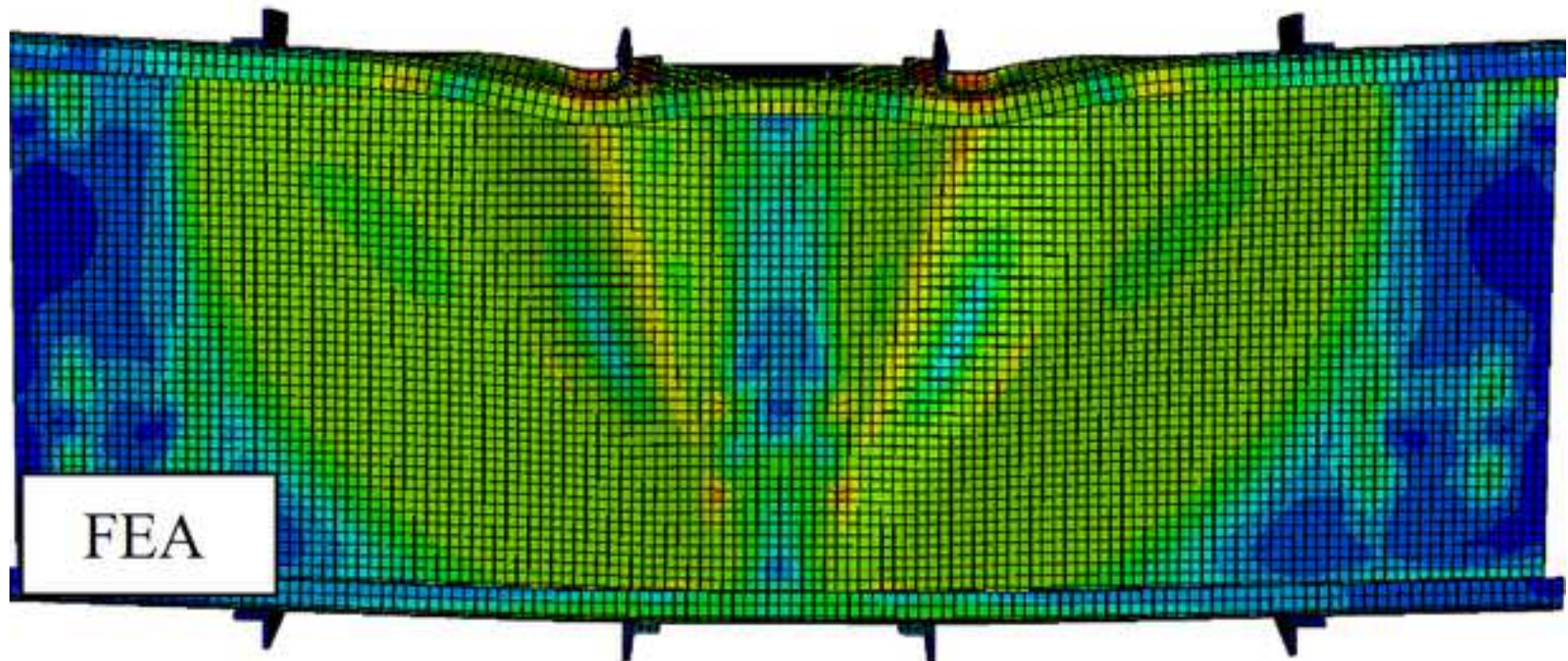
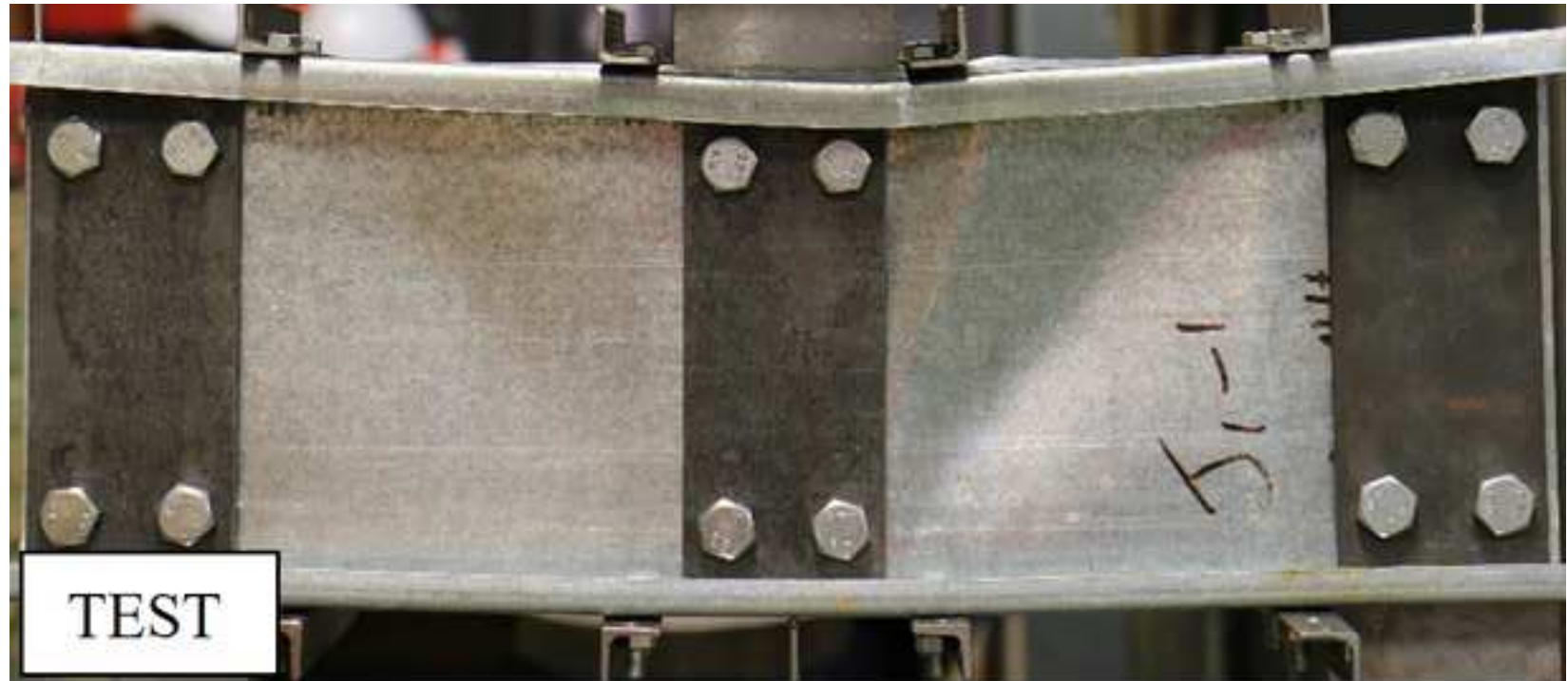




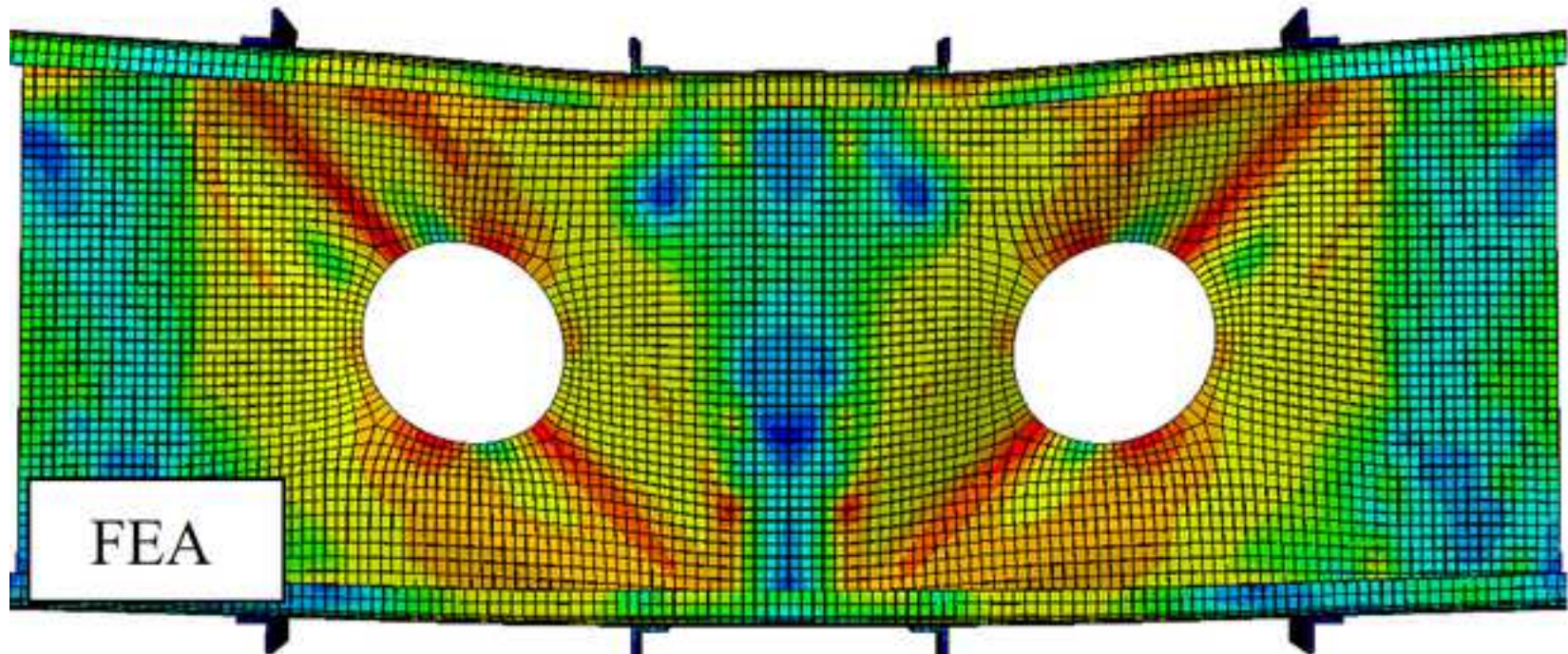
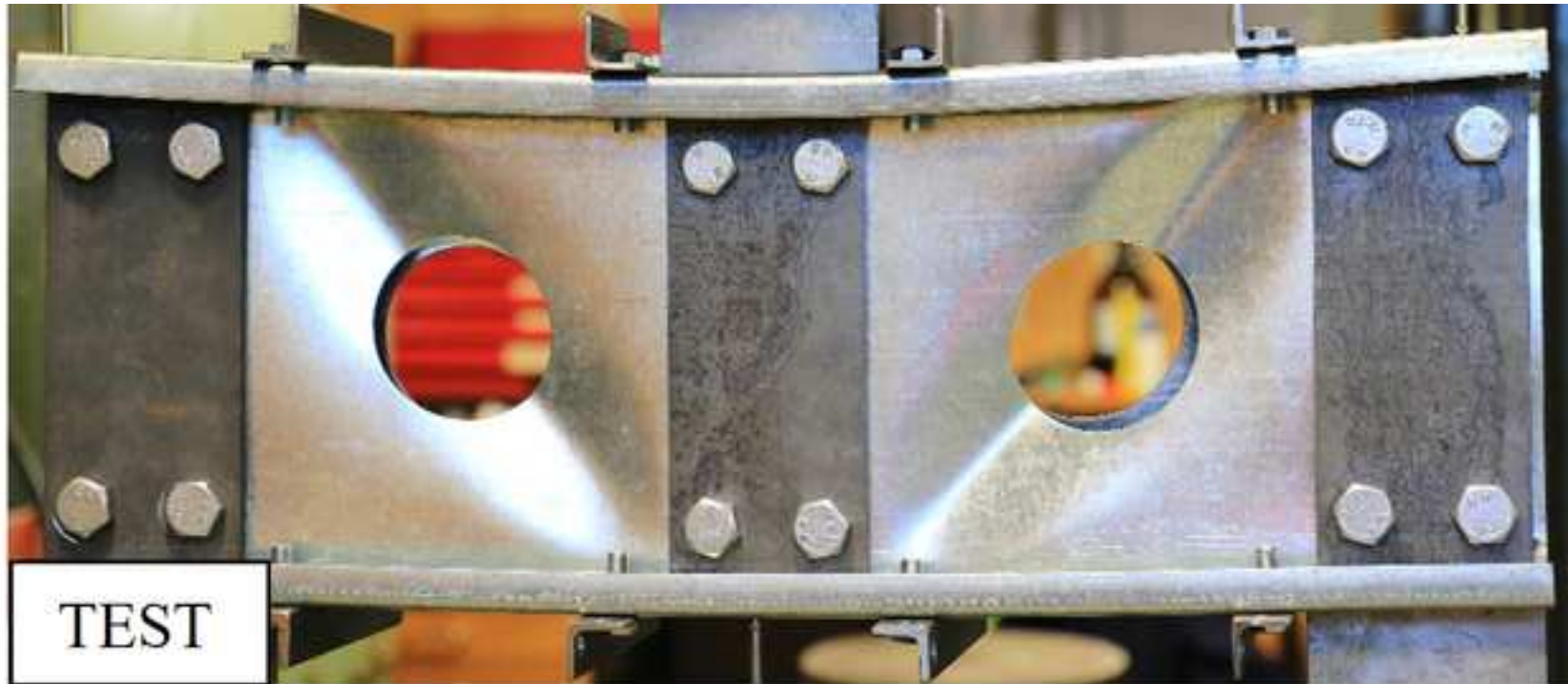




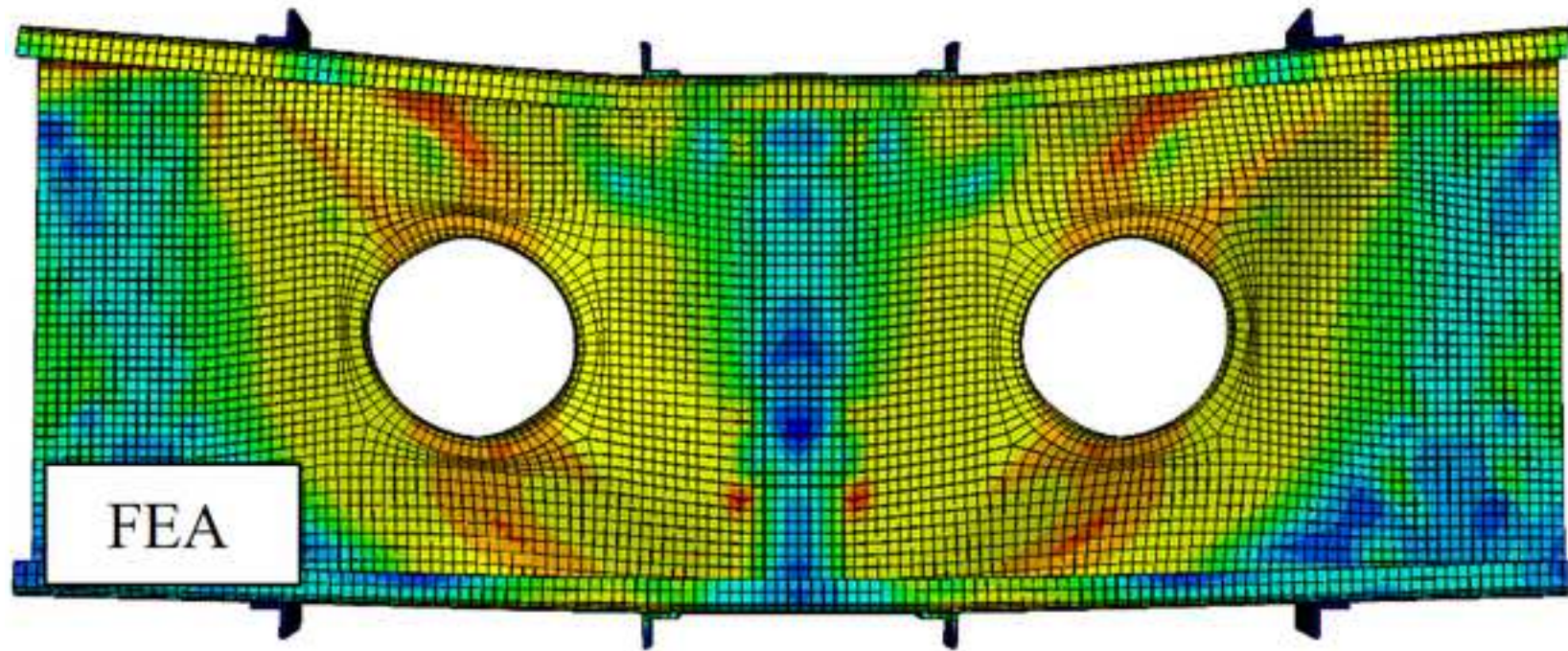
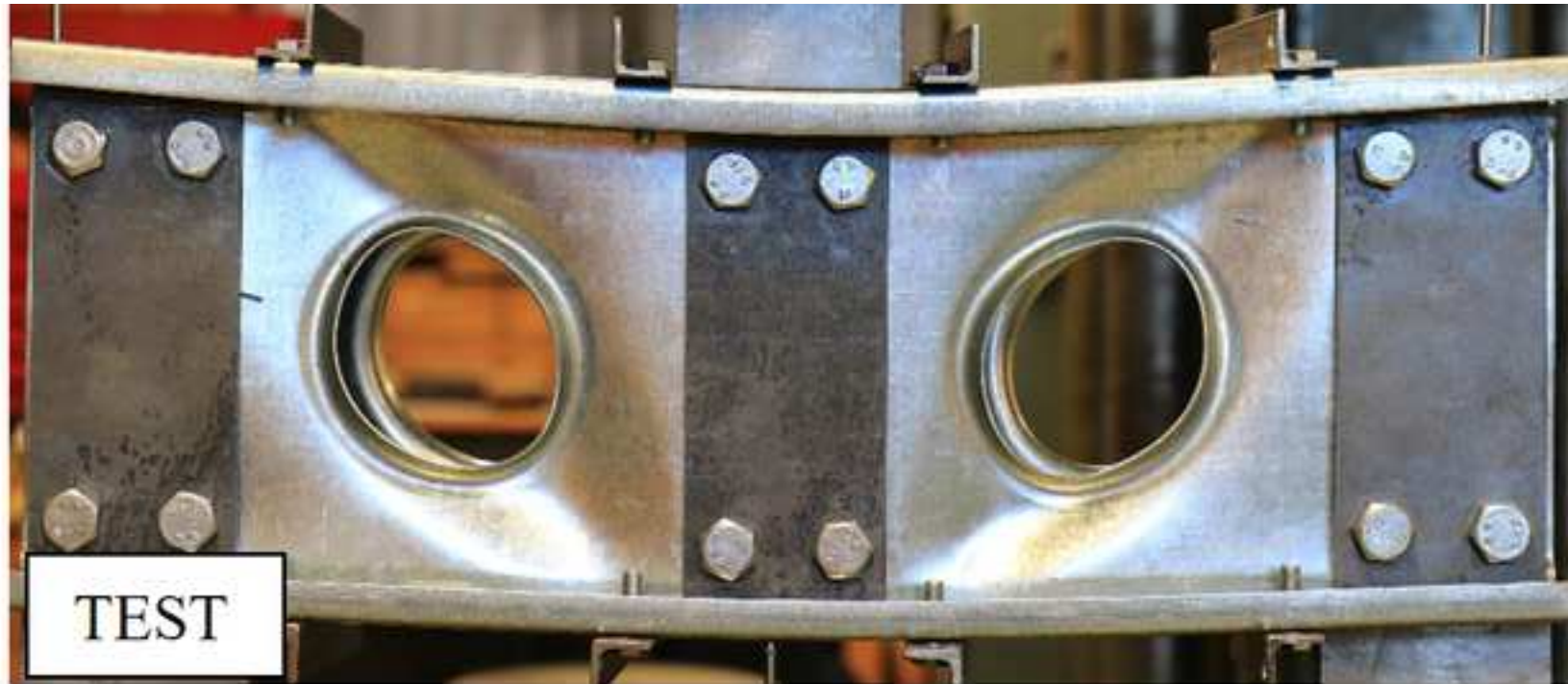




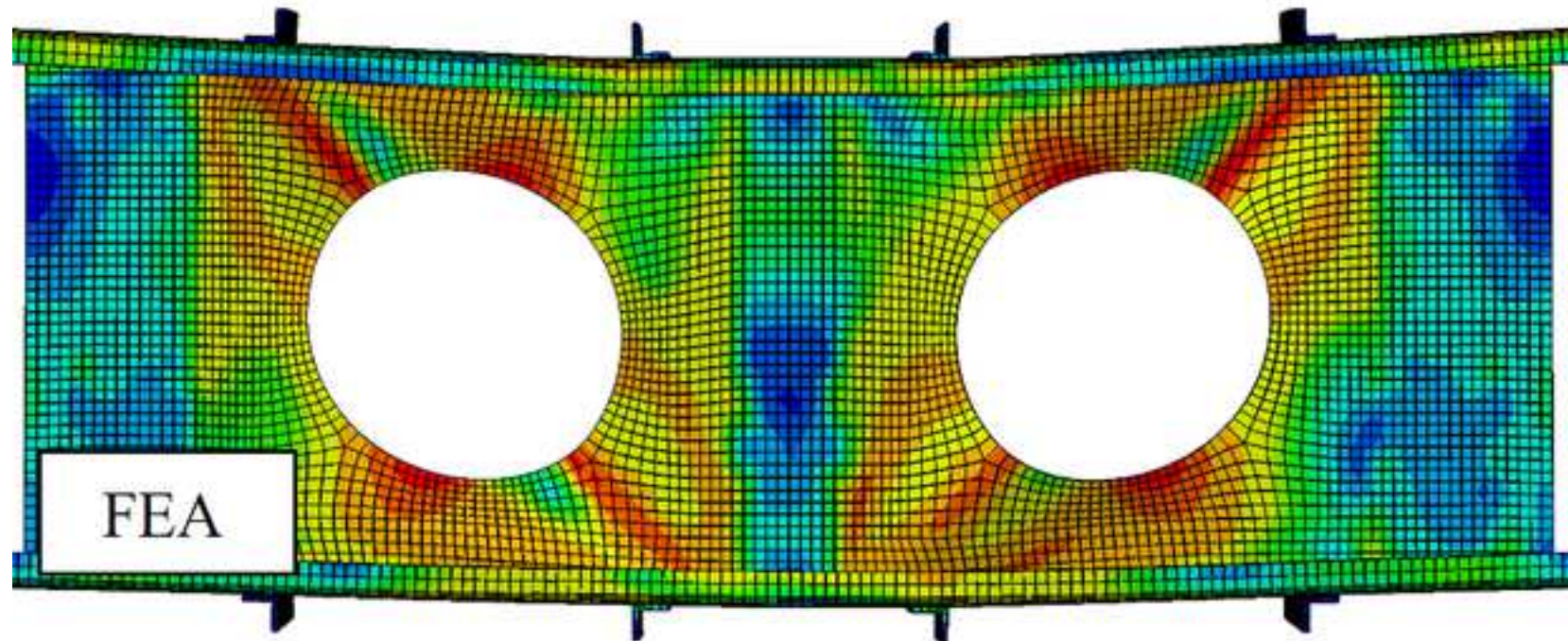
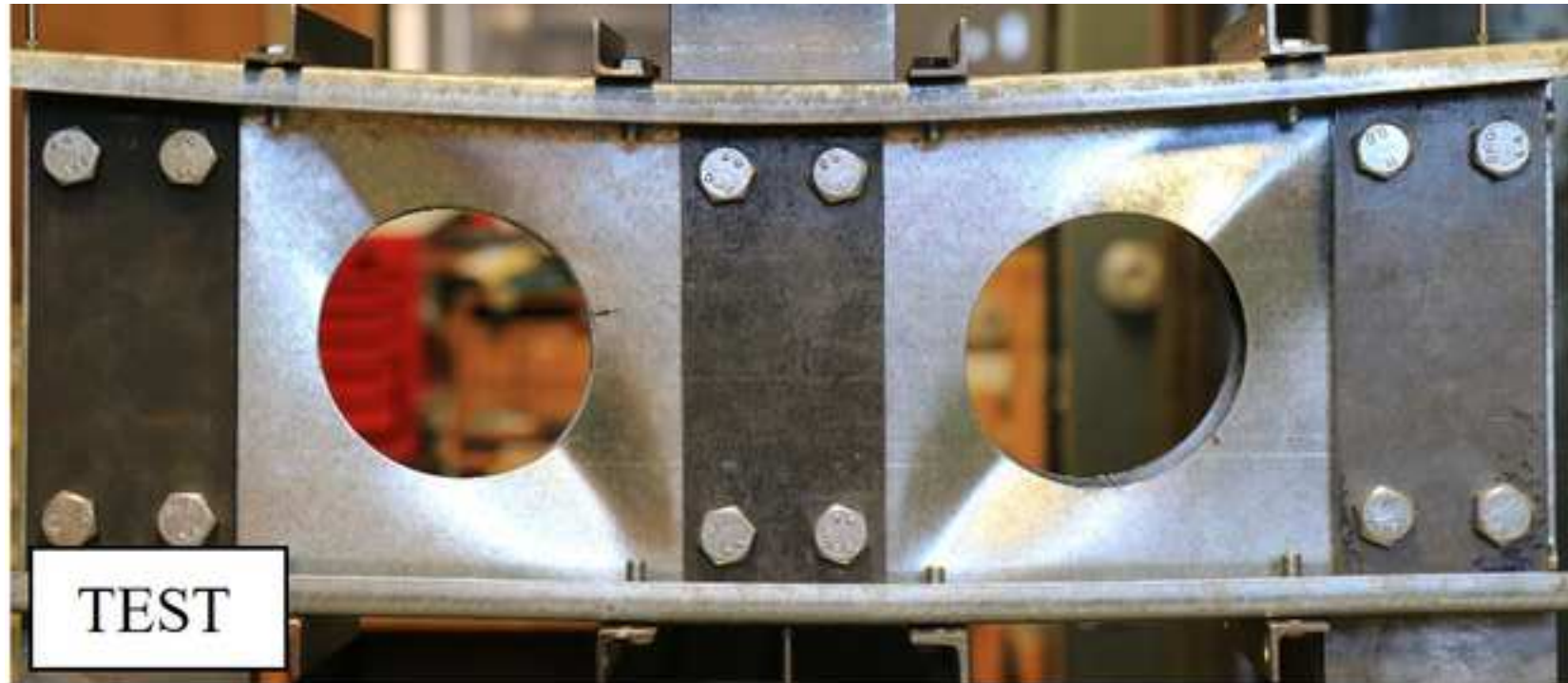




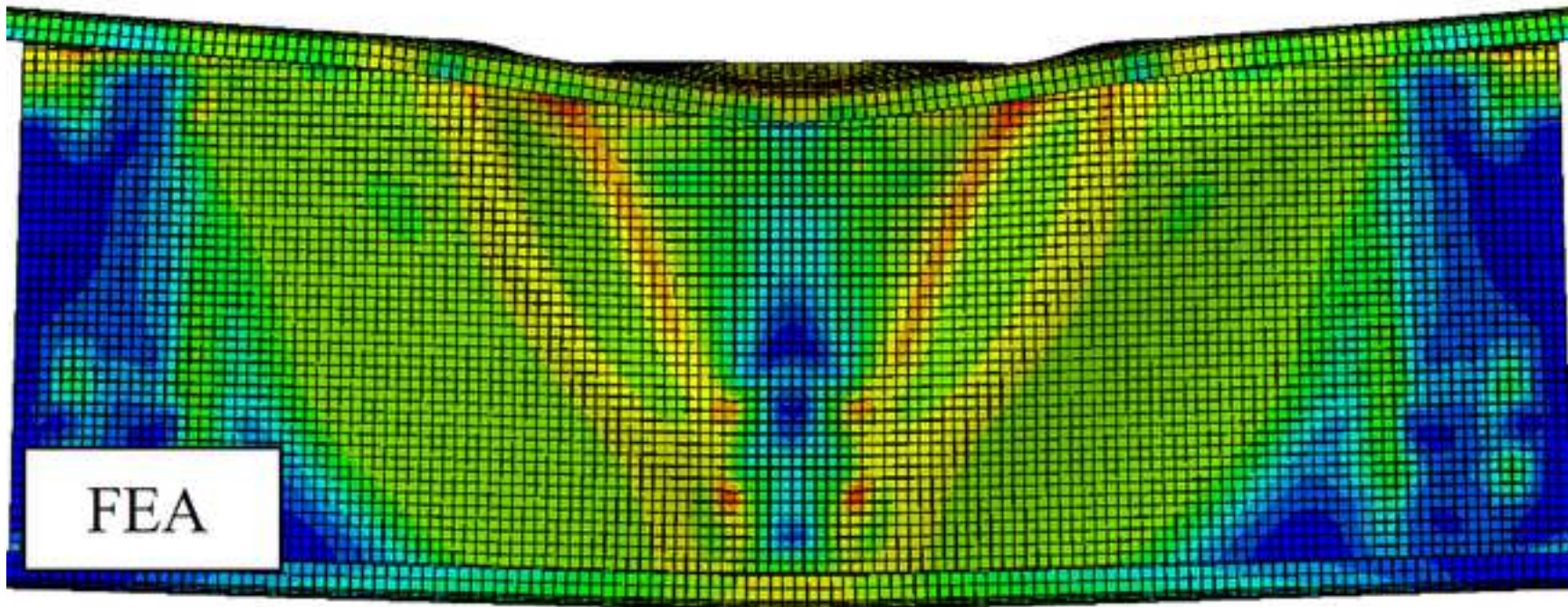
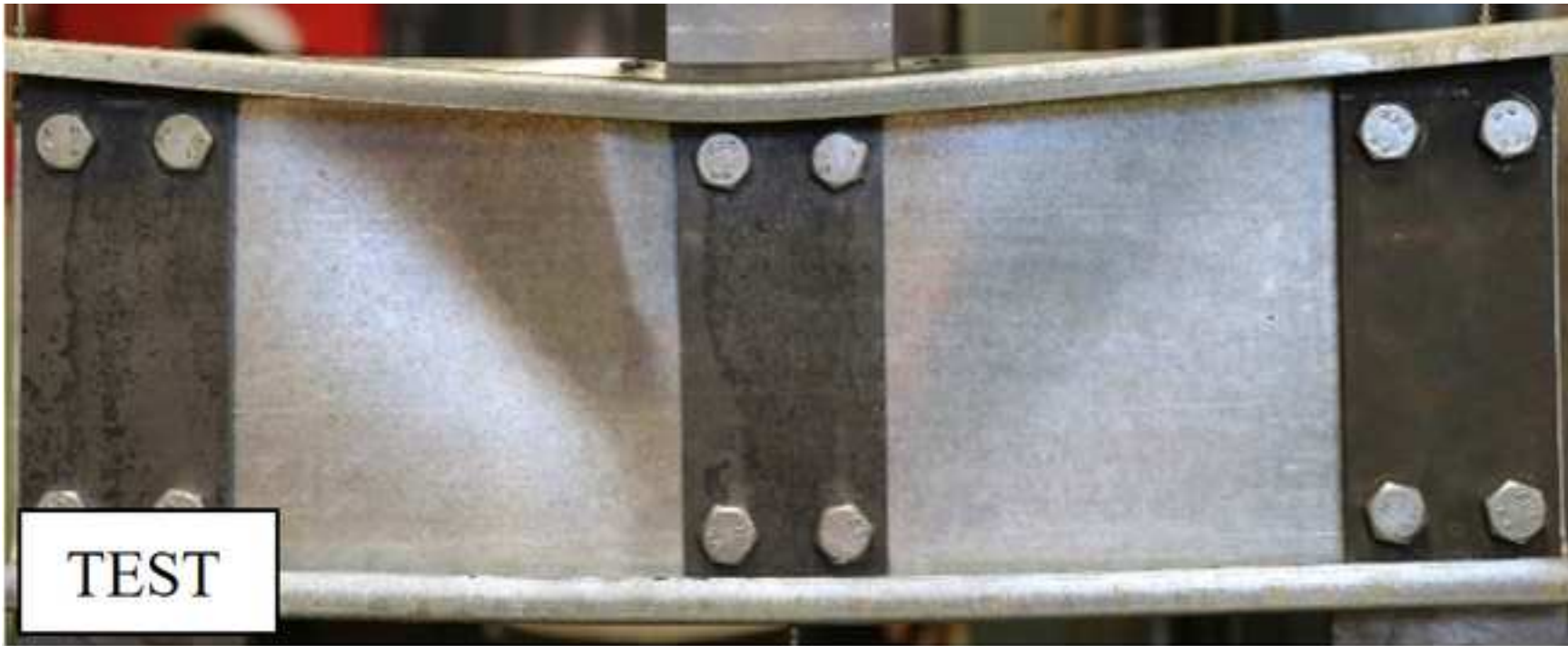




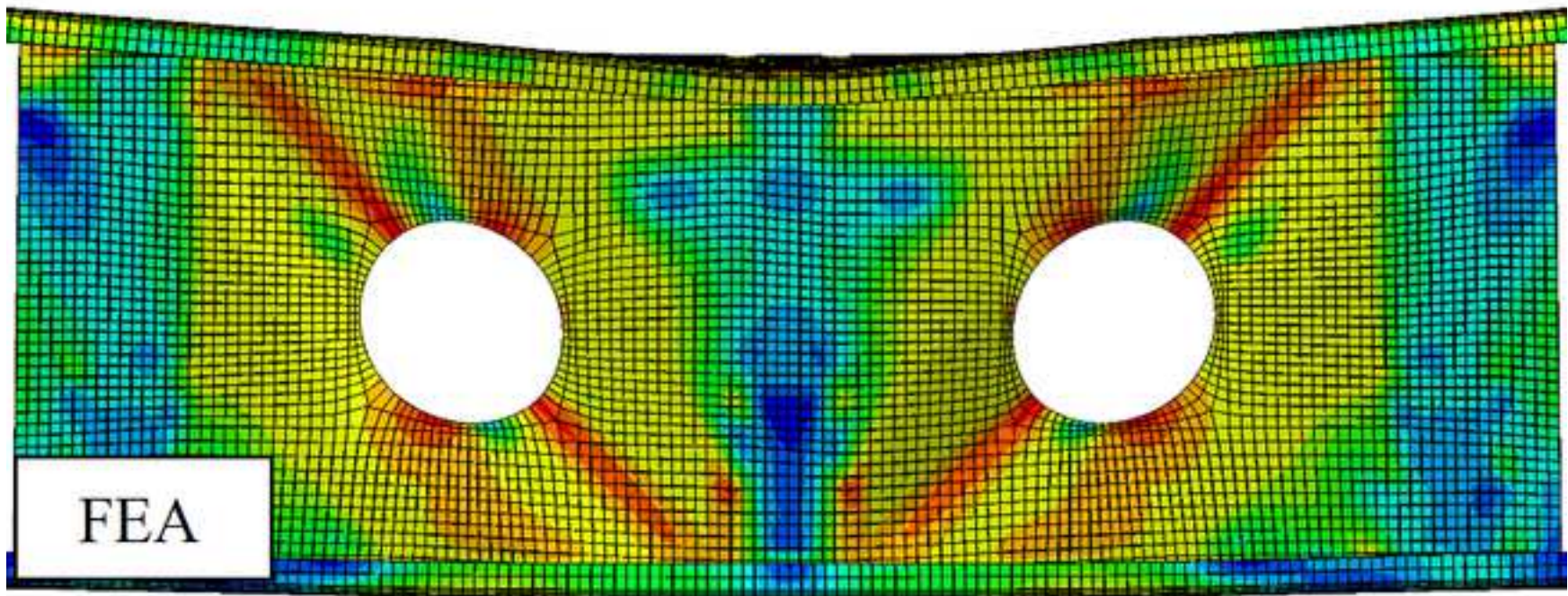
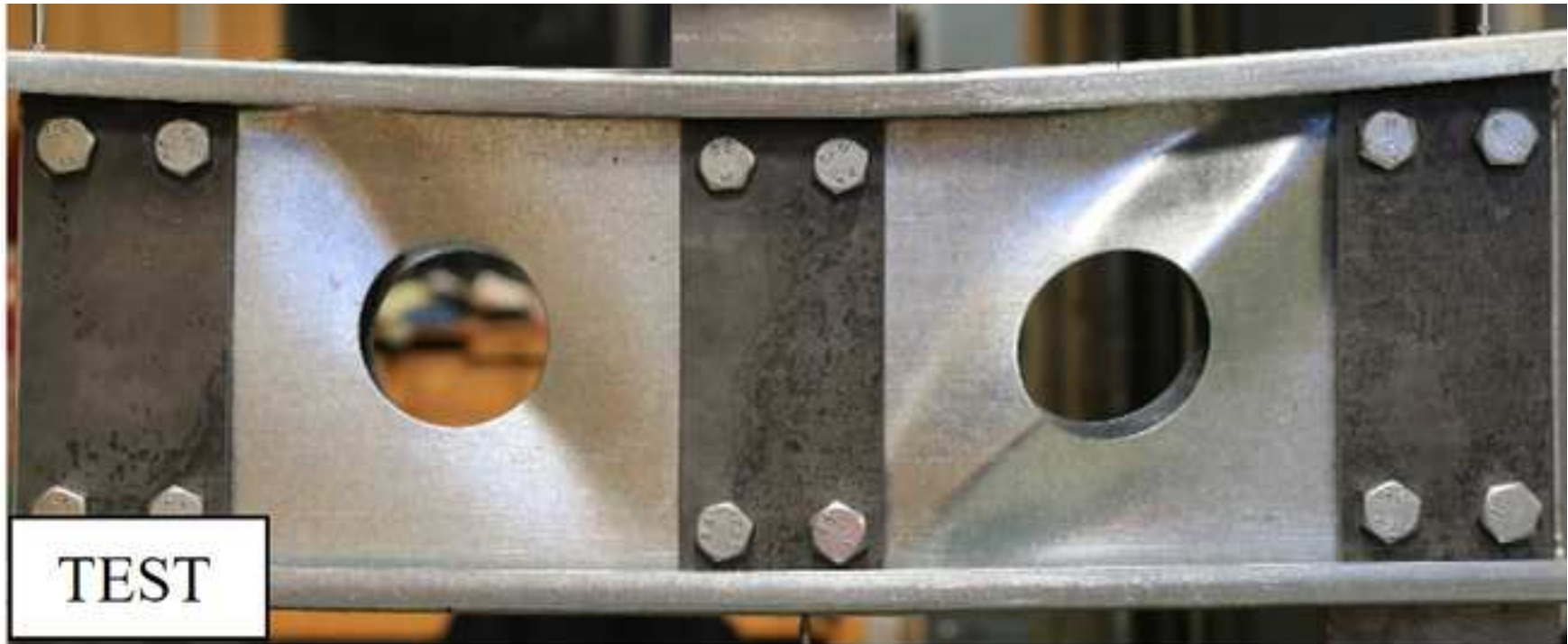




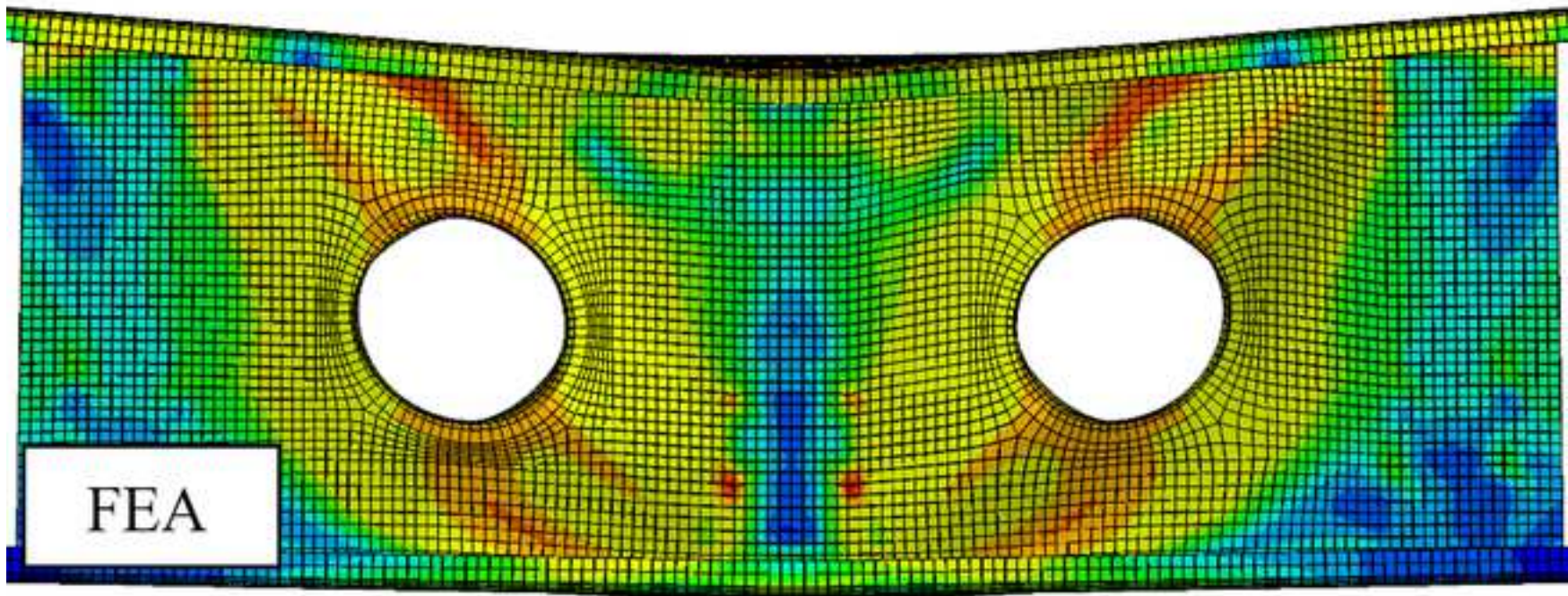




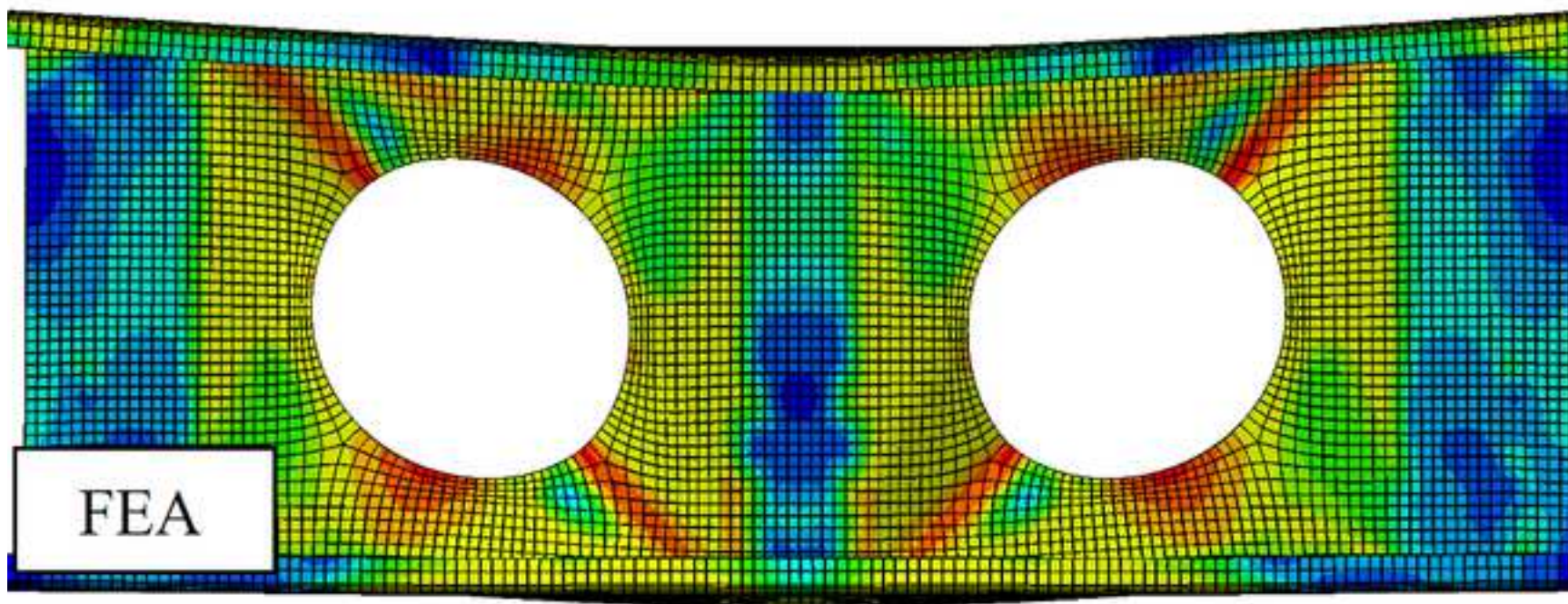


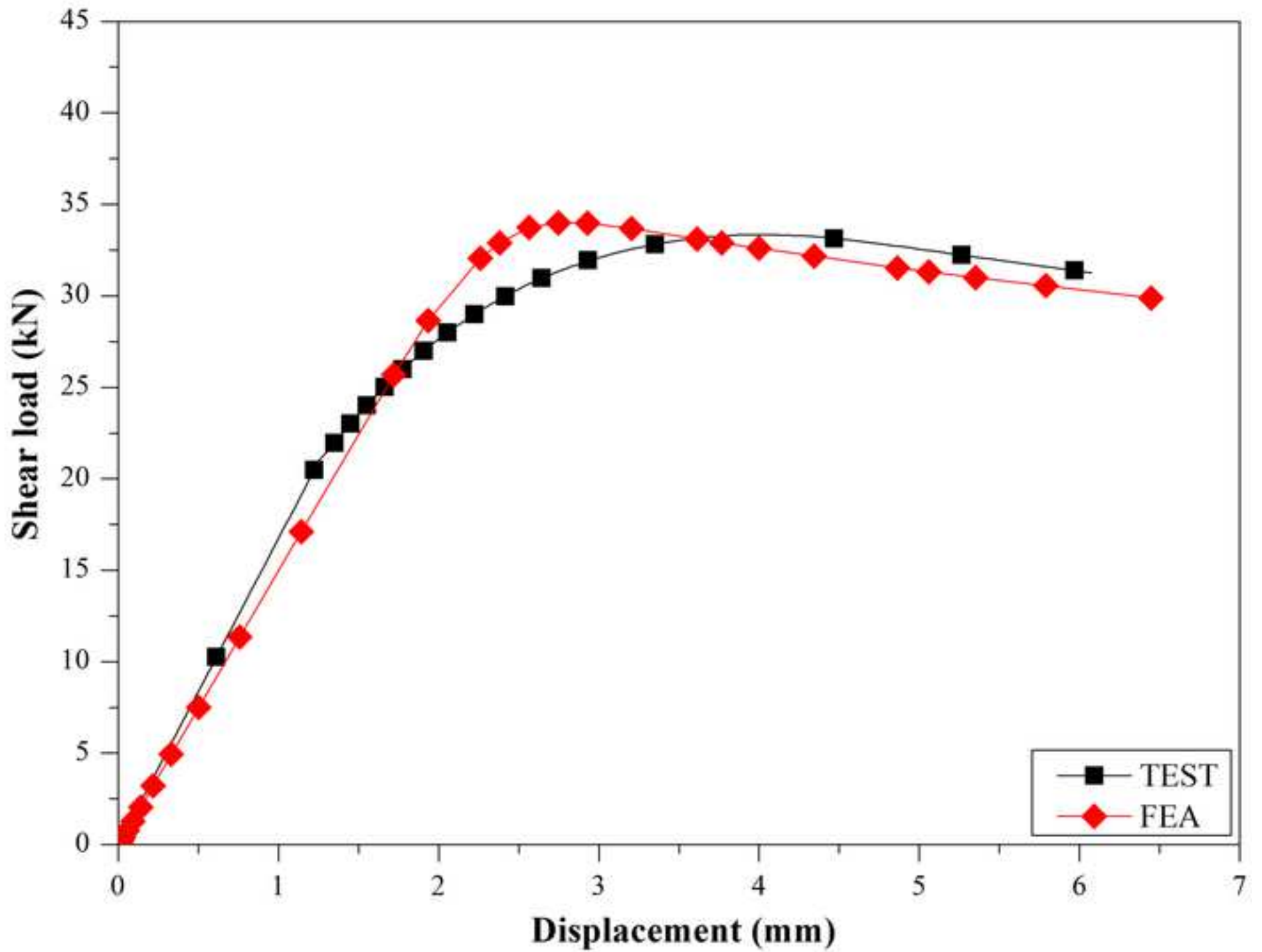


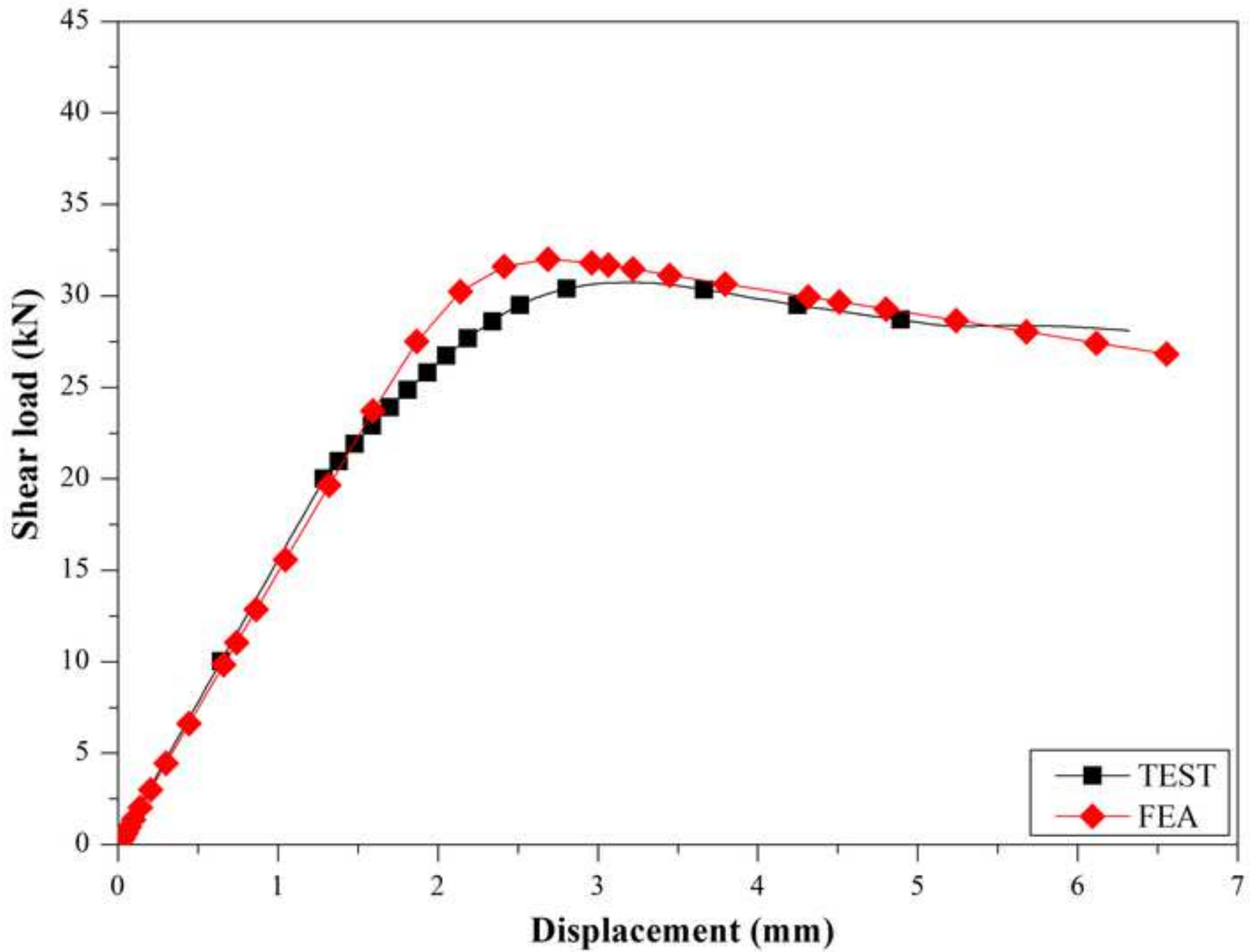


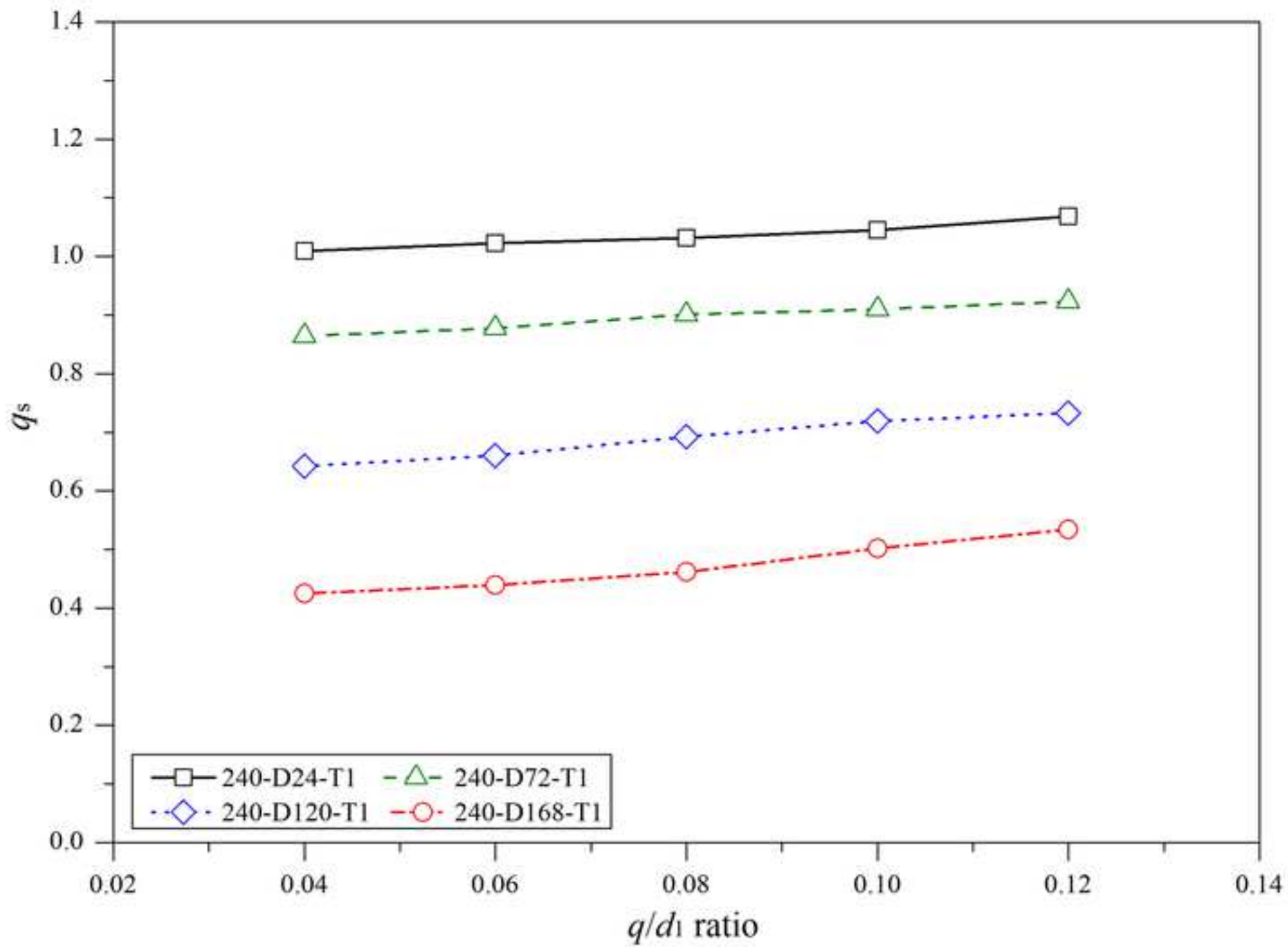




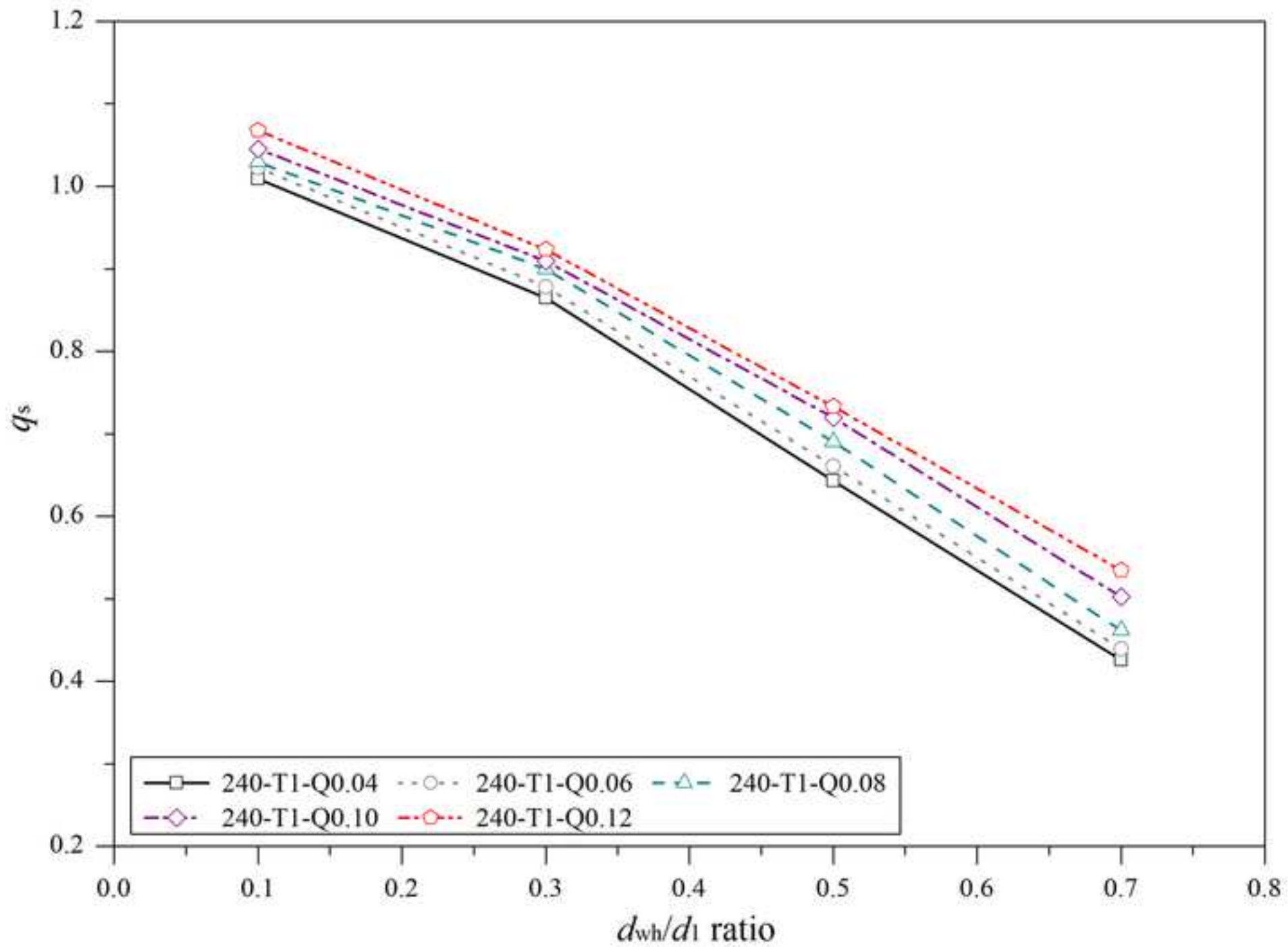


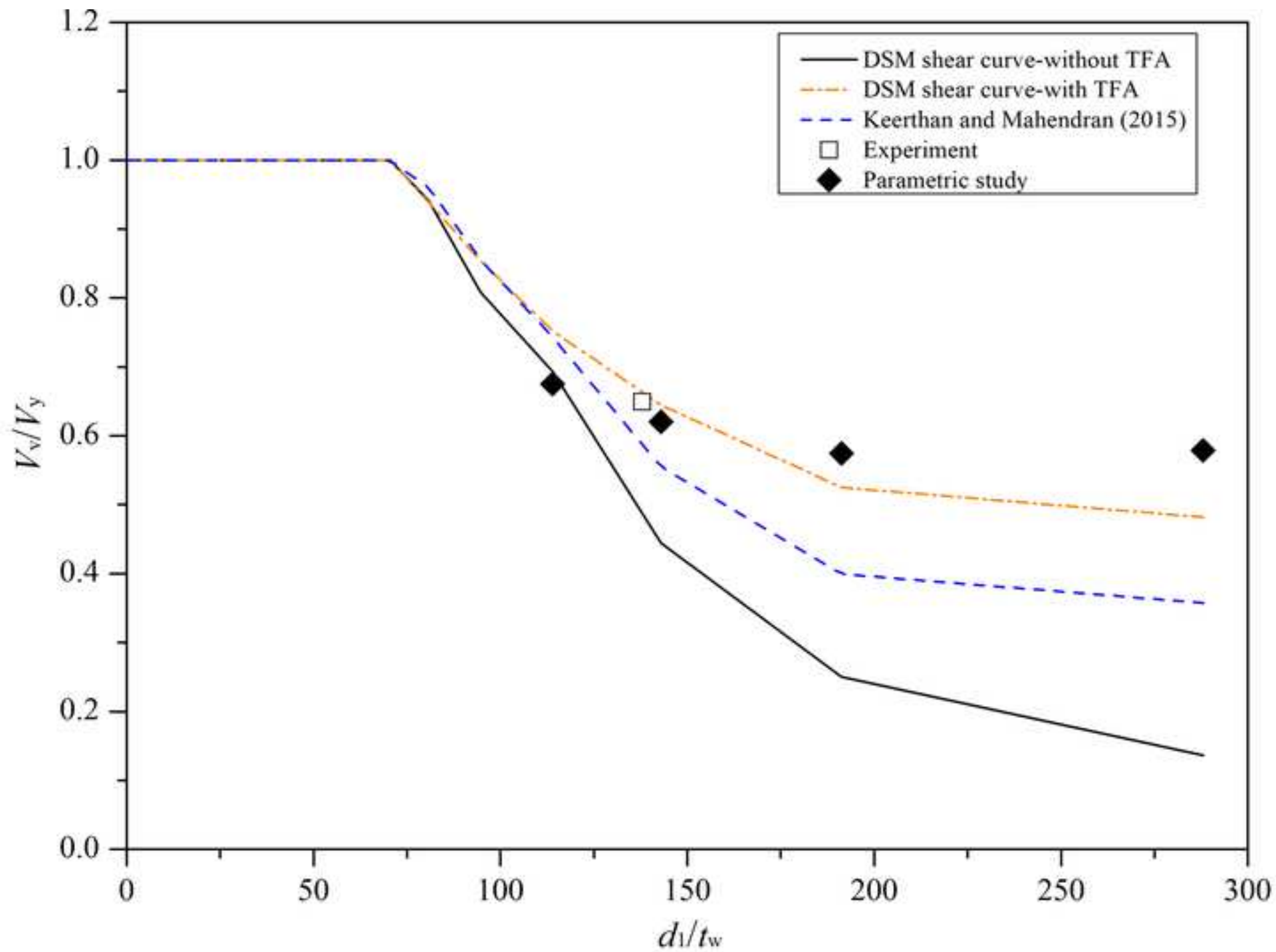


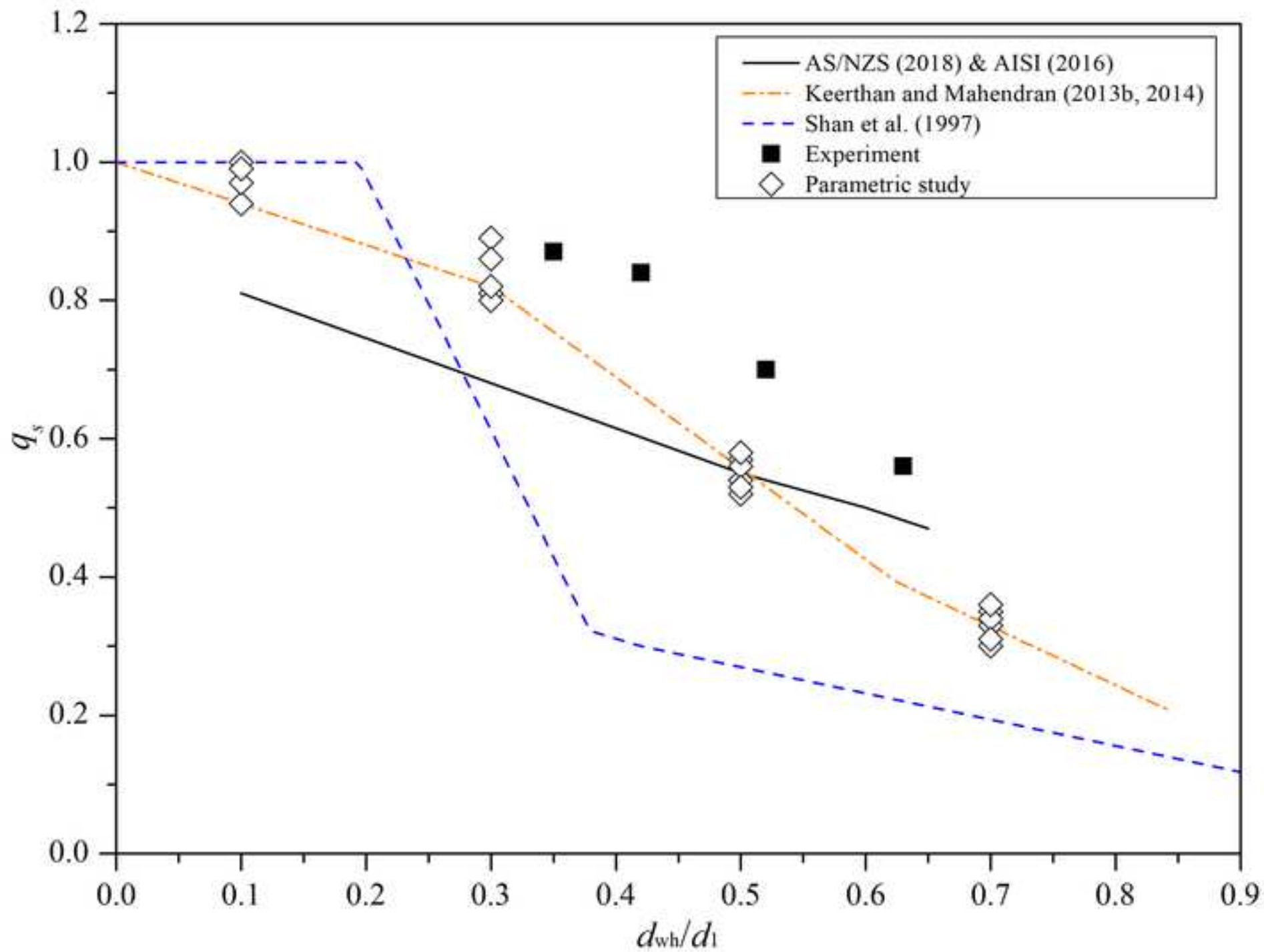


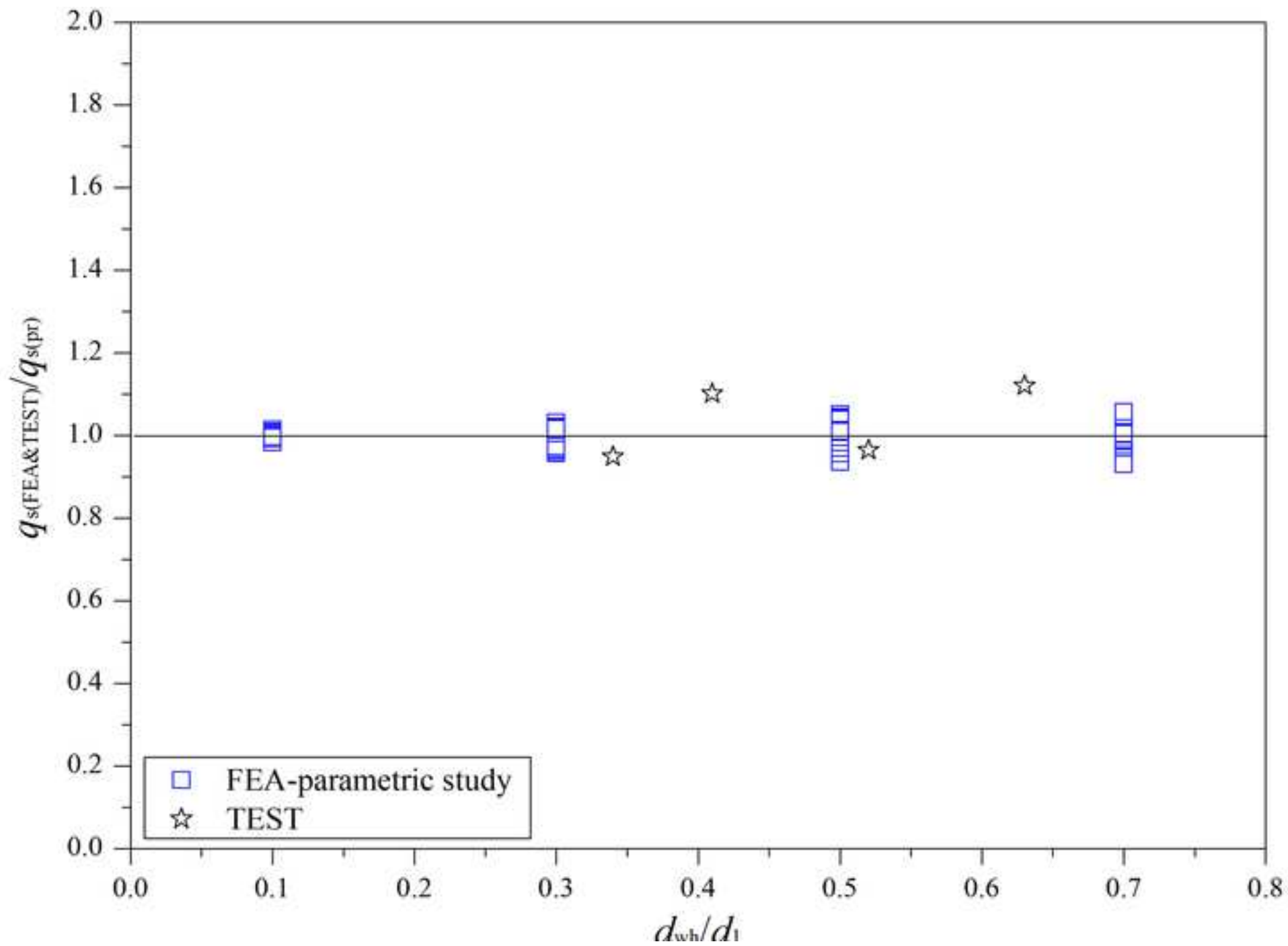














**List of figures**

Fig. 1 The use of cold-formed steel beams with edge-stiffened holes (Howick Ltd. 2013)

Fig. 2. Nominal cross-sections of the CFS channels considered in this paper.

(a) Section 240

(b) Section 290

Fig. 3. CFS channels studied in this paper

(a) CFS channels without holes

(b) CFS channels with un-stiffened web holes

(c) CFS channels with edge-stiffened web holes

Fig. 4. Experimental setup of tensile coupon test

Fig. 5. Stress-strain curves

(a) Section 240

(b) Section 290

Fig. 6. Photograph of test loading rig.

Fig. 7. Schematic drawing of loading rig

Fig. 8. Shear capacity versus displacement curves of all specimens

(a) section 240 with flange straps

(b) section 240 without flange straps

(c) section 290 with flange straps

Fig. 9. Failure modes of CFS channels with flange straps (aspect ratio=1.0)

(a) 240-A1.0-D0-NH-FR

(b) 240-A1.0-D140-UH-FR

(c) 240-A1.0-D140-EH-FR

Fig. 10. Failure mode of CFS channels without flange straps (240-A1.5-D0-NH-FU)

Fig. 11 Mesh type for specimen 290-A1.5-D140-EH-FR

Fig. 12 Boundary conditions within the FE model for specimen 290-A1.5-D140-EH-FR

Fig. 13. Effects of residual stresses (240-A1.5-D140-UH-FR)

Fig. 14. Deformed shapes at failure from experiments and FEA for those specimens with an aspect ratio of 1.0

(a) 240-A1.0-D0-NH-FR

(b) 240-A1.0-D90-UH-FR

(c) 240-A1.0-D140-EH-FR

(d) 240-A1.0-D140-UH-FR

(e) 240-A1.0-D0-NH-FU

(f) 240-A1.0-D90-UH-FU

(g) 240-A1.0-D140-EH-FU

(h) 240-A1.0-D140-UH-FU

Fig. 15. Comparison of FEA and experimental shear capacity versus displacement curves

(a) 240-A1.5-D90-UH-FR

(b) 240-A1.5-D90-UH-FU

Fig. 16. Effect of  $d_{wh}/d_1$  and  $q/d_1$  ratio on shear capacity reduction factor of channels with edge-stiffened web holes

(a) The effects of  $q/d_1$  ratio

(b) The effects of  $d_{wh}/d_1$  ratio

Fig. 17. Comparison of test and FEA results with current shear design strengths for plain channels

Fig. 18. Comparison of test and FEA results with current shear design rules for channels with un-stiffened web holes (aspect ratio=1.0)

Fig. 19. Comparison of test and FEA results with proposed reduction factor equations for channels with edge-stiffened web holes